

# Higgs Decays at NLO in the SMEFT

---

**Luigi Bellafronte,<sup>a</sup> Sally Dawson,<sup>b</sup> Clara Del Pio,<sup>b</sup> Matthew Forslund,<sup>c</sup> and Pier Paolo Giardino<sup>d</sup>**

<sup>a</sup>*Physics Department, Florida State University, Tallahassee, FL 32306-4350, USA*

<sup>b</sup>*High Energy Theory Group, Physics Department, Brookhaven National Laboratory, Upton, NY 11973, USA*

<sup>c</sup>*Princeton Center for Theoretical Science, Princeton University, Princeton, NJ, 08544 USA*

<sup>d</sup>*Departamento de Física Teórica and Instituto de Física Teórica UAM/CSIC, Universidad Autónoma de Madrid, Cantoblanco, 28049, Madrid, Spain*

*E-mail:* [lbellafronte@fsu.edu](mailto:lbellafronte@fsu.edu), [dawson@bnl.gov](mailto:dawson@bnl.gov), [celpio@bnl.gov](mailto:celpio@bnl.gov),  
[mforslund@princeton.edu](mailto:mforslund@princeton.edu), [pier.giardino@uam.es](mailto:pier.giardino@uam.es)

**ABSTRACT:** The calculation of precise predictions for Higgs decays is a necessary ingredient for determining Higgs properties at the LHC and future colliders. We compute all two- and three- body Higgs decays at next-to-leading order (NLO) in both QCD and electroweak interactions using the dimension-6 Standard Model Effective Field Theory (SMEFT). Results for four-body Higgs decays that are accurate to NLO QCD/electroweak order in the SMEFT are obtained using the narrow width approximation. Our results are contained in a flexible Monte Carlo program, NEWiSH, that is publicly available and we illustrate the impact of the NLO electroweak corrections for HL-LHC, Tera-Z, and Higgstrahlung projections.

NEWiSH is publicly available through [GitLab](https://gitlab.com/luigibellafronte/NEWiSH) .

---

## Contents

<b>1</b>	<b>Introduction</b>	<b>2</b>
<b>2</b>	<b>SMEFT NLO Calculation</b>	<b>4</b>
2.1	Renormalization	4
2.2	Real emission	7
2.3	Inputs	8
<b>3</b>	<b>Processes</b>	<b>9</b>
3.1	$h \rightarrow Z f \bar{f}$	10
3.2	$h \rightarrow W f \bar{f}'$	15
3.3	$h \rightarrow f \bar{f}$	18
3.4	$h \rightarrow VV'$	20
3.5	$h \rightarrow ggZ$	22
3.6	$h \rightarrow 4f$ and the narrow width approximation	22
<b>4</b>	<b>Results</b>	<b>25</b>
4.1	HL-LHC projections	25
4.2	Comparing Tera-Z reach with Higgstrahlung Sensitivity	27
4.3	Case Study: Scalar Singlet Model	29
<b>5</b>	<b>Conclusions</b>	<b>32</b>
<b>A</b>	<b>Code</b>	<b>43</b>
<b>B</b>	<b>Numerical results for <math>h \rightarrow f \bar{f}</math> and <math>h \rightarrow VV'</math></b>	<b>43</b>
B.1	$h \rightarrow l^+ l^-$	43
B.2	$h \rightarrow q \bar{q}$	45
B.3	$h \rightarrow \gamma \gamma$	48
B.4	$h \rightarrow \gamma Z$	49
B.5	$h \rightarrow gg$	49

## 1 Introduction

A precise understanding of Higgs boson interactions is central to the physics programs of present and future colliders. Currently, measurements of single Higgs production are in good agreement with theoretical predictions both for production and decay processes [1, 2]. With future high luminosity LHC (HL-LHC) measurements, however, the experimental uncertainties will be significantly reduced [3], requiring increasingly precise theoretical predictions.<sup>1</sup> Deviations from Standard Model (SM) predictions in the Higgs sector are further restricted by the lack of evidence for direct production of new particles which typically correspond to extensions of the Standard Model. It is thus reasonable to assume that any new physics corresponds to new interactions and/or new particles that are relevant at scales much larger than the electroweak scale.

The search for new physics can be systematically pursued using the Standard Model Effective Field Theory (SMEFT) [7]. This approach assumes that all Beyond the Standard Model (BSM) physics is at a very high scale compared to the weak scale and that the weak scale fields are those of the Standard Model interacting through an  $SU(3) \times SU(2) \times U(1)$  gauge symmetry. Furthermore, the SMEFT approach assumes that the electroweak symmetry breaking is linearly realized as in the SM and that the Higgs boson is part of an  $SU(2)$  doublet. The new physics can then be described as an expansion around the SM Lagrangian,

$$\mathcal{L} = \mathcal{L}_{\text{SM}} + \sum_{i,d} \frac{C_i^d}{\Lambda^{d-4}} O_i^d, \quad (1.1)$$

where  $\Lambda$  is the scale of the new physics and  $O_i^d$  are operators of dimension- $d$  containing only SM fields. All information about the nature of the new physics is contained in the coefficient functions,  $C_i^d$ .

The theory we have just described is a consistent field theory that admits a well-defined renormalization procedure, valid order by order in powers of  $\Lambda$ . In other words, once a specific power of  $\Lambda$  has been chosen, corrections to SM processes can be computed in a straightforward manner in terms of  $C_i^d/\Lambda^{d-4}$  and to any desired order in the loop expansion by consistently truncating higher powers of  $\Lambda$  that may appear in loop diagrams or when constructing physical observables. In our study we truncate the expansion at dimension-6 and we neglect the dimension-5 operators which generate lepton number violating interactions. At dimension-6, observables depend only on the ratio  $C/\Lambda^2$  and there is no independent sensitivity to the scale  $\Lambda$ .<sup>2</sup>

<sup>1</sup>See [4–6] for relevant summaries of current state of the art calculations in the Standard Model.

<sup>2</sup>We drop the superscript "6" in the remainder of this paper.

QCD corrections to one-loop order in the dimension-6 SMEFT are automated [8, 9] and can be calculated for all experimentally relevant processes. Higher order electroweak (EW) corrections in the SMEFT, however, need to be performed on a case-by-case basis. Numerous examples of electroweak dimension-6 SMEFT one-loop calculations exist:  $W$  and  $Z$  pole observables [10–12], Drell-Yan production [13, 14],  $e^+e^- \rightarrow Zh$  [15, 16], and many 2- and 3- body Higgs decays [17–28]. In this work, we summarize NLO results for all two- and three- body Higgs decays at one-loop in the CP conserving dimension-6 SMEFT, presenting new NLO results for the decays  $h \rightarrow Wff'$ ,  $h \rightarrow Zq\bar{q}$  and  $h \rightarrow Z\nu\bar{\nu}$ . Importantly, our results are contained in a public code that produces both total Higgs decay widths and distributions at one-loop in the SMEFT including all QCD and electroweak corrections. This code is part of a significant effort by many researchers to compute the Higgs production and decay channels that are measured at the LHC to one-loop electroweak order in the SMEFT to facilitate a global fit that is accurate to this order.<sup>3</sup> The calculations are also crucial for the study of Higgstrahlung and  $Z$  pole observables at future  $e^+e^-$  colliders.

At one-loop order in the SMEFT, a plethora of operators typically contribute to observables, with the exact number depending on the underlying flavor assumptions. For example,  $Z$  and  $W$  pole observables (EWPOs) at leading order (tree) depend on 10 dimension-6 operators, while at next-to-leading order (one-loop), the number increases to 32 in the scenario where flavor is ignored. Assuming a  $U(2)^5$  scenario, for example, the number of operators contributing to EWPOs increases to 93 [10, 30]. In this work, we combine previous one-loop electroweak SMEFT results for  $e^+e^- \rightarrow Zh$  [15, 16] with our NLO results for  $h \rightarrow X$ , where  $X$  is a two- or three- body final state. All possible flavor interactions are included in the calculation, however we drop contributions proportional to the off-diagonal elements of the Cabibbo-Kobayashi-Maskawa (CKM) matrix. To recover the four fermion final state we use combinations of full results and the narrow width approximation (NWA), as described in Sec. 3.6.

In Sec. 2, we present a detailed discussion of the SMEFT one-loop electroweak calculation of Higgs decays and the dipole subtraction used to regulate the real photon and gluon emission contributions. We then discuss each Higgs decay individually in Sec. 3, including numerical results for the widths. In Sec. 4, we present some numerical examples of the impact of our work including partial NLO projections for the sensitivities for Higgs processes at the HL-LHC. We give a comparison of sensitivities at Tera-Z and HL-LHC to selected operators that occur at loop level and hence would be omitted in tree level SMEFT studies. As a case study of the impact of NLO electroweak corrections in the SMEFT, we demonstrate the sensitivity of the Higgs singlet model to NLO corrections and emphasize the impact of the model assumptions on the projections. The use of our public code NEWiSH [31] for the study of one-loop dimension-6 SMEFT operators in Higgs decays is detailed in an appendix.

---

<sup>3</sup>An important and still missing piece for a complete NLO description of SMEFT processes are the two-loop SMEFT renormalization group equations (RGE). The bosonic two-loop contributions are known [29].

## 2 SMEFT NLO Calculation

We begin by establishing our conventions and discussing the details of our calculations, first broadly and then individually for each process. The starting point is the dimension-6 SMEFT Lagrangian Eq. (1.1) in the Warsaw basis [32, 33]. We do not assume any specific flavor structure for the operators that can appear in our calculation. However, the CKM matrix is taken to be diagonal, to restrict the flavour structures that appear in any given process.

We obtain the amplitudes that contribute to the virtual one-loop corrections using the chain FEYNRULES [34]→FEYNARTS [35]→ FEYNCALC [36]. The resulting Feynman integrals, which we calculate using  $D = 4 - 2\epsilon$  dimensional regularization, are expressed in terms of Passarino-Veltman functions [37], whose analytical and numerical expressions we obtain from PACKAGE-X [38] and COLLIER [39]. For all processes, we take as input parameters

$$M_W, M_Z, G_\mu, m_h, m_t, \alpha_S, \quad (2.1)$$

where the masses are on-shell, and the Fermi constant  $G_\mu$  is determined from the decay of the muon. The masses of leptons and quarks (excluding the top quark), are generally taken to be zero. However, for the Higgs decays into light fermions,  $h \rightarrow f\bar{f}$ , we also include the masses of second and third generation quarks when their impact is sufficiently large. We leave the details to the respective sections.

Phase space integration is handled via a public Fortran code NEWISH  [31] that we describe in App. A. The calculation of the three-body decays mirrors that of [15, 16, 26] for  $\ell^+\ell^-Z$ , extended to include the  $q\bar{q}Z$ ,  $\nu\bar{\nu}Z$ , and  $f\bar{f}'W^\pm$  processes. For three-body decay processes  $h \rightarrow f\bar{f}'V$  ( $V = W, Z$ ), we take all fermions massless except for the top-quark.<sup>4</sup>

For  $h \rightarrow f\bar{f}$  decays, in order to have a consistent SM contribution, light fermion masses need to be included. In this context, adopting an  $\overline{\text{MS}}$  rather than an on-shell definition of the input masses makes a significant numerical difference, as we discuss in Sec. 3.3.1. For the  $h \rightarrow f\bar{f}$  decays, since the mediating vector bosons can be on-shell, we adopt the complex mass scheme for the treatment of the unstable particles [40, 41].

To obtain predictions for the four-body decays  $h \rightarrow (f_1\bar{f}_2)(f_3\bar{f}_4)$  at NLO in the SMEFT, we use the narrow width approximation (NWA) with our  $h \rightarrow f\bar{f}'V$  NLO decay calculation and the known results for  $W$  and  $Z$  decays at NLO [10, 11]. At lowest order (LO), we calculate the full four-body process with no approximation and employ the complex mass scheme, which ensures a gauge-invariant description of the off-shell vector bosons. We discuss the narrow width approximation in more detail in Sec. 3.6.<sup>5</sup>

### 2.1 Renormalization

We calculate our results employing two different renormalization conditions for the counterterms. In the first approach, we use the on-shell (OS) scheme for the SM parameters,

<sup>4</sup>With the exception of in some differential distributions – see Sec. 3.1.1 for details.

<sup>5</sup>Some of the pitfalls of the NWA at tree level in the SMEFT are discussed in [42].

while the  $\overline{\text{MS}}$  scheme is used for the renormalization of SMEFT operators. The second approach is very similar to the first, however the masses of the light quarks (i.e all excluding the top quark), are calculated in the  $\overline{\text{MS}}$  scheme. As usual, we define the OS quantities in terms of the masses of the bosons and fermions, with the addition of the Fermi constant  $G_\mu$ . We note that  $e$  is not an independent parameter of the model, ( $e$  is defined as the coupling of the electron to the photon in SMEFT). It is convenient to express the electromagnetic coupling in terms of our input parameters as

$$e^2 = G_\mu \sqrt{2} (1 + X_H) 4 M_W^2 \left( 1 - \frac{M_W^2}{M_Z^2} \right) - \frac{2 M_W^3}{M_Z^2 \Lambda^2} \left\{ M_W C_{\phi D} + 4 \sqrt{M_Z^2 - M_W^2} C_{\phi WB} \right\} + \mathcal{O}\left(\frac{1}{\Lambda^4}\right), \quad (2.2)$$

where at dimension-6

$$X_H \equiv \frac{1}{\sqrt{2} G_\mu \Lambda^2} \left\{ C_{ll}[1221] - C_{\phi l}^{(3)}[11] - C_{\phi l}^{(3)}[22] \right\}. \quad (2.3)$$

The indices in the square brackets are generation indices.

We fix the tadpole renormalization by setting tadpole contributions to zero [43]. This approach corresponds to equating the renormalized vacuum expectation value (VEV) of the Higgs field to the minimum of the renormalized scalar potential. The relation between the renormalized VEV  $v$  and  $G_\mu$  is then given by,

$$\sqrt{2} G_\mu (1 + X_H) = \frac{1}{v^2} (1 + \Delta r). \quad (2.4)$$

The function  $\Delta r$  [44, 45] has been calculated in the SMEFT at dimension-6 in [21]. Notice that, due to our choice of tadpole scheme,  $\Delta r$  is a gauge-dependent quantity. We use the gauge-dependence of our intermediate calculations to check the correctness of the final result. Specifically, we explicitly check the gauge independence of the result for the SM calculation and for specific parts of the SMEFT calculation, as checking the gauge invariance of the full SMEFT calculation is impractical due to the large size of the amplitudes involved.

The renormalization conditions for the masses of the vector bosons  $V$  ( $V = W, Z$ ) are set by the definitions

$$M_V^2 = M_{0,V}^2 - \delta M_V^2, \quad (2.5)$$

which relate the bare mass  $M_{0,V}^2$  to the physical mass  $M_V^2$ .  $\delta M_V^2$  are the mass counterterms and, at one-loop, are defined by the relations

$$\delta M_V^2 = \text{Re}(\Pi_{T,VV}(M_V^2)), \quad (2.6)$$

where  $\Pi_{T,VV}(M_V^2)$  are the transverse parts of the one-loop corrections to the two-point functions evaluated at the physical mass  $M_V^2$ . Notice that, following the standard definition,

we take the real part of the two-point functions. We will see in Sec. 3.3 that we need to use a complex mass scheme for the  $h \rightarrow f\bar{f}$  decays due to a divergence in the real corrections to those processes when the  $Z$  boson propagator goes on-shell. However, since vector bosons do not contribute at LO in those decays we do not need to alter our renormalization procedure.

For the Higgs boson, the renormalization condition is very similar, and we define

$$m_h^2 = m_{0,h}^2 - \delta m_h^2, \quad \delta m_h^2 = \text{Re}(\Pi_{hh}(m_h^2)) \quad (2.7)$$

where, again,  $m_{0,h}$  and  $m_h$  are the bare and physical masses of the Higgs boson, respectively, and  $\Pi_{hh}(m_h^2)$  is the one-loop correction to the Higgs boson two-point function evaluated at the physical Higgs mass.

For the fermions it is convenient to first define the fermionic two-point function, which we write as

$$\Sigma(p) = \frac{1 - \gamma_5}{2}(\not{p}\Sigma_{p,L} + \Sigma_{m,L}) + \frac{1 + \gamma_5}{2}(\not{p}\Sigma_{p,R} + \Sigma_{m,R}), \quad (2.8)$$

where  $p$  is the momenta of the fermion. The relation between the bare fermionic mass  $m_{0,f}$  and physical mass  $m_f$  then becomes

$$m_f^2 = m_{0,f}^2 - \delta m_f^2, \quad (2.9)$$

where

$$\delta m_f^2 = m_f^2(\Sigma_{p,L} + \Sigma_{p,R}) + m_f(\Sigma_{m,L} + \Sigma_{m,R}). \quad (2.10)$$

These formulas are valid in both the OS and  $\overline{\text{MS}}$  schemes; the only distinction is whether one subtracts the full function or only its divergent part, respectively.

Regarding the wave-function renormalization, we have the following definitions:

$$\begin{aligned} \delta Z_{\gamma\gamma} &= -\frac{d\Pi_{\gamma\gamma}}{dp^2}\bigg|_{p^2=0}, \quad \delta Z_{VV} = -\frac{d\Pi_{VV}}{dp^2}\bigg|_{p^2=M_V^2}, \quad \delta Z_h = -\frac{d\Pi_{hh}}{dp^2}\bigg|_{p^2=m_h^2}, \\ \delta Z_{f,L} &= -\Sigma_{p,L} + 2\frac{d}{dp^2}(m_f^2\Sigma_{m,L} + m_f\Sigma_{p,L})\bigg|_{p^2=m_f^2}, \\ \delta Z_{f,R} &= -\Sigma_{p,R} + 2\frac{d}{dp^2}(m_f^2\Sigma_{m,R} + m_f\Sigma_{p,R})\bigg|_{p^2=m_f^2}. \end{aligned} \quad (2.11)$$

Additional wave-function renormalization counterterms come from the requirement that off-diagonal  $\gamma - Z$  mixing terms vanish at the poles, from which we have

$$\delta Z_{\gamma Z} = -2\frac{\Pi_{\gamma Z}(M_Z^2)}{M_Z^2}, \quad \delta Z_{Z\gamma} = 2\frac{\Pi_{\gamma Z}(0)}{M_Z^2}, \quad (2.12)$$

where  $\Pi_{\gamma Z}$  is the contribution from the two-point Feynman diagram which mixes photons and  $Z$  bosons.

Finally, as advertised at the beginning of the section, we renormalize the bare dimension-6 SMEFT coefficients,  $C_{0,i}$ , in the  $\overline{\text{MS}}$  scheme

$$C_i(\mu) = C_{0,i} - \frac{1}{2\hat{\epsilon}} \frac{1}{16\pi^2} \gamma_{ij} C_j(\mu), \quad (2.13)$$

where  $\hat{\epsilon}^{-1} \equiv \epsilon^{-1} - \gamma_E + \log(4\pi)$ ,  $\mu$  is the renormalization scale, and  $\gamma_{ij}$  are the elements of the anomalous dimension matrix [46–49], that is

$$16\pi^2 \frac{dC_i(\mu)}{d\ln\mu} = \gamma_{ij} C_j(\mu). \quad (2.14)$$

Coefficients in our numerical expressions for the widths are evaluated at the scale  $\mu = m_h$  and we do not include the RGE running of the coefficients needed to match to models at the scale  $\Lambda$  [50, 51].

## 2.2 Real emission

Infrared (IR) divergences in the virtual amplitudes are canceled by real photon or real gluon emission,  $h \rightarrow X + \gamma/g$ . We treat these using standard dipole subtraction techniques, as described in [43, 52–54]. Depending on the process, we require a combination of massive [53, 54] and massless [43, 52] dipole subtraction. Explicitly, for the real emission contribution, we have

$$\Gamma_{\text{Real}} = \frac{1}{2m_h} \int dPS_n (|\mathcal{A}_{\text{R}}|^2 - |\mathcal{A}_{\text{sub}}|^2) + \int d\Gamma_{\text{sub}} \quad (2.15)$$

where  $|\mathcal{A}_{\text{R}}|^2$  is the amplitude squared for the real emission process  $H \rightarrow X + \gamma/g$ , expanded to  $\mathcal{O}(1/\Lambda^2)$ . Since all of our splittings are of the form  $X \rightarrow \gamma/g(p_i) + X(p_j)$  with spectator particle momentum  $p_k$  and final-state emission only, the subtraction kernel  $|\mathcal{A}_{\text{sub}}|^2$  is given by (see Sec. 5 of [54])

$$|\mathcal{A}_{\text{sub}}|^2 = -8\pi\alpha_S C_F \sum_{\langle jk \rangle} |\mathcal{A}_{\text{LO}}(p_j \rightarrow \tilde{p}_{ij}, p_k \rightarrow \tilde{p}_k)|^2 \frac{1}{(p_i + p_j)^2 - m_j^2} \quad (2.16)$$

$$\times \left\{ \frac{2}{1 - \tilde{z}_j(1 - y_{ij,k})} - \frac{\tilde{v}_{ij,k}}{v_{ij,k}} \left[ 1 + \tilde{z}_j + \frac{m_j^2}{p_i \cdot p_j} \right] \right\}, \quad (2.17)$$

where the sum is over emitter-spectator pairs  $\langle jk \rangle$ ,  $m_{i\dots k}^2 = (p_i + \dots + p_k)^2$ , and  $\mathcal{A}_{\text{LO}}$  is the leading order amplitude for  $h \rightarrow X$  expanded to  $\frac{1}{\Lambda^2}$ . For real photon emission one replaces  $4\pi\alpha_S C_F \rightarrow e^2 Q_j Q_k$  with  $Q_j$  the electric charge of particle  $j$  and  $e$  the QED gauge coupling expanded to  $\frac{1}{\Lambda^2}$  in terms of the input parameters, as defined in Eq. (2.2). The new variables in Eq. (2.16) are given by

$$\tilde{z}_j = \frac{p_i \cdot p_k}{(p_i \cdot p_k + p_j \cdot p_k)}, \quad y_{ij,k} = \frac{p_i \cdot p_j}{p_i \cdot p_j + p_i \cdot p_k + p_j \cdot p_k} \quad (2.18)$$

$$\tilde{v}_{ij,k} = \frac{\lambda^{1/2}(m_{ijk}^2, m_j^2, m_k^2)}{m_{ijk}^2 - m_j^2 - m_k^2}, \quad (2.19)$$

$$v_{ij,k} = \frac{\sqrt{[2m_k^2 + (m_{ijk}^2 - m_j^2 - m_k^2)(1 - y_{ij,k})]^2 - 4m_{ijk}^2 m_k^2}}{(m_{ijk}^2 - m_j^2 - m_k^2)(1 - y_{ij,k})}, \quad (2.20)$$

where  $\lambda(a, b, c)$  is the usual Källén triangle function. The LO amplitude  $|\mathcal{A}_{\text{LO}}(\tilde{p}_{ij}, \tilde{p}_k)|^2$  in Eq. (2.16) is evaluated with momenta  $\tilde{p}_{ij}$  and  $\tilde{p}_k$  given by

$$\begin{aligned} \tilde{p}_k^\mu &= \frac{\lambda^{1/2}(m_{ijk}^2, m_j^2, m_k^2)}{\lambda^{1/2}(m_{ijk}^2, m_j^2, m_k^2)} \left( p_k^\mu - \frac{p_{ijk} \cdot p_k}{m_{ijk}^2} p_{ijk}^\mu \right) + \frac{p_{ijk}^2 - m_k^2 - m_j^2}{2m_{ijk}^2} p_{ijk}^\mu \\ \tilde{p}_{ij}^\mu &= p_{ijk}^\mu - \tilde{p}_k^\mu \end{aligned} \quad (2.21)$$

where  $p_{ijk}^\mu \equiv p_i^\mu + p_j^\mu + p_k^\mu$ . In the massless limit,  $m_j, m_k \rightarrow 0$ , these formulas reproduce the massless case in [43]. We will however need the full mass dependence for the  $h \rightarrow f\bar{f}$  and  $h \rightarrow f\bar{f}'W^\pm$  processes described below.

The subtracted piece is integrated analytically using dimensional regularization and added back as  $\int d\Gamma_{\text{sub}}$ , given explicitly by

$$d\Gamma_{\text{sub}} = \frac{1}{2m_h} dPS_{n-1} \frac{\alpha_S}{2\pi} C_F \sum_{\langle jk \rangle} |\mathcal{A}_{\text{LO}}|^2 \left( 2I_+^{\text{eik}} + I_{gQ,k}^{\text{coll}} \right), \quad (2.22)$$

where the integrals  $I_+^{\text{eik}}$  and  $I_{gQ,k}^{\text{coll}}$  are given in Eqs. 5.34 and 5.35 in [54].

It should be kept in mind that the dipole subtraction formulae written here are valid only for inclusive observables. For a non-inclusive observable such as  $d\Gamma/dm_{\ell\ell}$  for  $h \rightarrow \ell^+ \ell^- Z$ , the lepton mass  $m_\ell$  enters as a regulator and additional terms appear. See Sec. 3.1.1 for details.

The total decay width is then the sum of the real and virtual pieces described above.

### 2.3 Inputs

In the numerical results that follow, we use a renormalization scale  $\mu = m_h$  to define the observables and a SMEFT scale  $\Lambda = 1$  TeV. We take as our inputs [55]

$$\begin{aligned} M_W &= 80.352 \text{ GeV} \\ M_Z &= 91.1535 \text{ GeV} \\ G_\mu &= 1.16638 \times 10^{-5} \text{ GeV}^{-2} \\ m_h &= 125.1 \text{ GeV} \\ m_t &= 172.76 \text{ GeV} \\ \alpha_S(m_h) &= 0.1188 \\ \Delta\alpha_{\text{had}} &= 0.02768. \end{aligned} \quad (2.23)$$

The vector boson masses denote here the pole definitions [55, 56]

$$M_V = \frac{M_V^{\text{exp}}}{\sqrt{1 + (\Gamma_V^{\text{exp}}/M_V^{\text{exp}})^2}}, \quad (2.24)$$

and correspond to experimental values of  $M_W^{\text{exp}} = 80.379$  GeV,  $M_Z^{\text{exp}} = 91.1876$  GeV,  $\Gamma_W^{\text{exp}} = 2.085$  GeV,  $\Gamma_Z^{\text{exp}} = 2.4952$  GeV. For the  $h \rightarrow f\bar{f}$  processes, we take the additional on-shell inputs [57]

$$\begin{aligned} m_\tau &= 1.777 \text{ GeV} \\ m_\mu &= 0.1057 \text{ GeV} \\ m_e &= 0.511 \times 10^{-3} \text{ GeV} \\ m_b &= 4.92 \text{ GeV} \\ m_c &= 1.51 \text{ GeV} \\ m_s &= 0.1 \text{ GeV}, \end{aligned} \tag{2.25}$$

where only masses  $m_f \geq m_{f_i}$  are taken to be nonzero for each  $h \rightarrow f_i\bar{f}_i$  channel. See the description of each individual process below for more detail. For  $h \rightarrow q\bar{q}$ , we additionally show numerical results using  $\overline{\text{MS}}$  input values [58],

$$\begin{aligned} m_b^{\overline{\text{MS}}}(m_b) &= 4.183 \text{ GeV} \\ m_c^{\overline{\text{MS}}}(m_c) &= 1.273 \text{ GeV} \\ m_s^{\overline{\text{MS}}}(2 \text{ GeV}) &= 0.0935 \text{ GeV}. \end{aligned} \tag{2.26}$$

### 3 Processes

In this section, we discuss the different two- and three- body processes that contribute to the Higgs width at NLO QCD and EW in the dimension-6 SMEFT and our implementation in NEWiSH.<sup>6</sup> With the exceptions of  $h \rightarrow VV'$  with  $VV' \in (gg, \gamma\gamma, Z\gamma)$  and  $h \rightarrow ggZ$  which are loop induced in the SM, the LO plus one-loop virtual amplitudes for the decay processes  $h \rightarrow X$  are given by

$$\mathcal{A}(h \rightarrow X) = \mathcal{A}_{\text{SM}}^{(0)} + \frac{1}{\Lambda^2} \mathcal{A}_{\text{EFT}}^{(0)} + \frac{1}{(4\pi)^2} \mathcal{A}_{\text{SM}}^{(1)} + \frac{1}{(4\pi\Lambda)^2} \mathcal{A}_{\text{EFT}}^{(1)} + \dots \tag{3.1}$$

where we truncate everywhere at  $\mathcal{O}(\frac{1}{16\pi^2\Lambda^2})$ . The LO plus virtual  $h \rightarrow X$  amplitudes-squared are then simply

$$\begin{aligned} |\mathcal{A}_{\text{Virt}}|^2 = & |\mathcal{A}_{\text{SM}}^{(0)}|^2 + \frac{2}{\Lambda^2} \text{Re} \left( \mathcal{A}_{\text{SM}}^{(0)*} \mathcal{A}_{\text{EFT}}^{(0)} \right) \\ & + \frac{2}{(4\pi)^2} \text{Re} \left( \mathcal{A}_{\text{SM}}^{(0)*} \mathcal{A}_{\text{SM}}^{(1)} \right) + \frac{2}{(4\pi\Lambda)^2} \text{Re} \left( \mathcal{A}_{\text{SM}}^{(0)*} \mathcal{A}_{\text{EFT}}^{(1)} + \mathcal{A}_{\text{SM}}^{(1)*} \mathcal{A}_{\text{EFT}}^{(0)} \right) + \dots \end{aligned} \tag{3.2}$$

where the first line is LO and the second is part of the NLO correction <sup>7</sup>.

---

<sup>6</sup>We neglect a handful of ultrarare decays described in [59] that are also vanishingly small in the SMEFT at  $\mathcal{O}(1/\Lambda^2)$ .

<sup>7</sup>We should emphasize that we always truncate the amplitude squared  $|\mathcal{A}|^2$  at  $\mathcal{O}(1/\Lambda^2)$ . Consistently including all  $\mathcal{O}(1/\Lambda^4)$  contributions to an observable requires both double insertions of dimension-6 operators and the inclusion of dimension-8 operators to ensure UV pole cancellation and gauge invariance [60, 61].

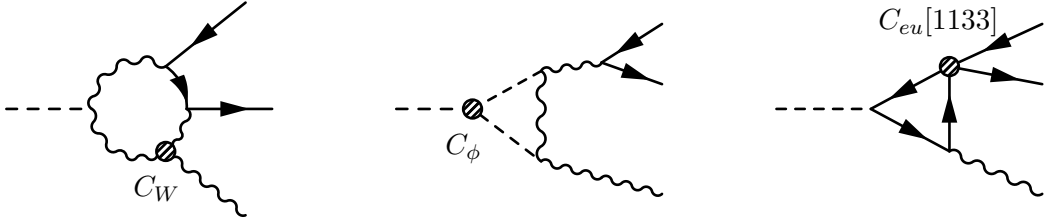


**Figure 1.** Representative diagrams for virtual contributions to the  $h \rightarrow f\bar{f}Z$  decay process in the SMEFT.

The total NLO widths also require contributions from real photon and gluon emission, as discussed in Section 2.2. The relevant amplitudes squared for the  $h \rightarrow X + \gamma/g$  processes are given by

$$|\mathcal{A}(h \rightarrow X + \gamma/g)|^2 = |\mathcal{A}_{X+\gamma/g, \text{SM}}^{(0)}|^2 + \frac{2}{\Lambda^2} \text{Re} \left[ \mathcal{A}_{\text{SM}, X+\gamma/g}^{(0)*} \mathcal{A}_{\text{EFT}, X+\gamma/g}^{(0)} \right] + \dots \quad (3.3)$$

For each process, we present numeric results for the total NLO partial width  $\Gamma_{\text{NLO}}(h \rightarrow X)$  with the inputs of Sec. 2.3 in the form  $\Gamma_{\text{NLO}} = \Gamma_{\text{LO}} + \delta\Gamma_{\text{NLO}}$ , where  $\Gamma_{\text{LO}}$  is the leading order contribution in the dimension-6 SMEFT and  $\delta\Gamma_{\text{NLO}}$  is the total NLO correction. We drop coefficients with negligibly small contributions, though full numerical results for each process including all contributions can be found in the GitLab repository [31]. We now consider each process in more detail.

### 3.1 $h \rightarrow Z f\bar{f}$

In the SM, the  $h \rightarrow Z f\bar{f}$  processes are contained in the full  $h \rightarrow 4f$  decays, which are known at NLO QCD and EW order in the SM [62–65]. The SM corrections most relevant for  $h \rightarrow Z f\bar{f}$  are conveniently implemented in PROPHECY4F [66], HTO4L [62], and HDECAY [67].

In the SMEFT, only  $h \rightarrow Z\ell^+\ell^-$  ( $\ell = \mu, e$ ) is known to one-loop, as described in detail in [26]. Here we extend that calculation to include  $h \rightarrow Z\tau^+\tau^-$ ,  $h \rightarrow Z\nu\bar{\nu}$  and  $h \rightarrow Zq\bar{q}$  using the same methodology. Sample diagrams contributing to the virtual contributions are shown in Fig. 1. As discussed above, we consider all fermions massless except for  $m_t$ , although the lepton masses enter as a regulator in non-inclusive observables in  $h \rightarrow Z\ell^+\ell^-$ . We do not include the effects of finite  $W$  and  $Z$  widths in either the real emission or the virtual amplitudes since the  $Z$  appears as an external state <sup>8</sup>.

#### 3.1.1 $h \rightarrow Z\ell^+\ell^-$

The  $h \rightarrow Z\ell^+\ell^-$  process gives us access to semi-leptonic and fully leptonic  $h \rightarrow 4f$  decays in the narrow width approximation. Since  $h \rightarrow 4\ell$  is particularly important at the LHC,

<sup>8</sup>In a full  $h \rightarrow 4f$  calculation one could impose the complex mass scheme as we do in  $h \rightarrow f\bar{f}$ . We do this for our leading order predictions in Sec. 3.6, but it is inconsistent at NLO when using the narrow width approximation.

we have also implemented  $m_{\ell\ell}$  cuts and the non-inclusive differential distribution  $d\Gamma/dm_{\ell\ell}$  for this channel<sup>9</sup>.

To include non-inclusive observables, an additional term is required in the dipole subtraction procedure. This term is described in [26] and we write it here for completeness. In the notation of [43], this amounts to using in Eq. (2.15)

$$|\mathcal{A}_{\text{sub}}|^2 = 2e^2 \frac{p_{\ell^+} \cdot p_{\ell^-}}{(p_{\ell^+} \cdot p_\gamma)(p_{\ell^-} \cdot p_\gamma)} \quad (3.4)$$

$$\begin{aligned} \int d\Gamma_{\text{sub}}^{h \rightarrow Z\ell^+\ell^-} = & \left[ \int d\widetilde{\text{PS}}_3 |\mathcal{A}_{\text{LO}}|^2 \int_0^1 dz \left\{ G^{(\text{sub})}(\tilde{m}_{\ell\ell}^2) \delta(1-z) + [\bar{\mathcal{G}}_{\text{MR}}(\tilde{m}_{\ell\ell}^2, z)]_+ \right\} \right. \\ & \left. \times \Theta_{\text{cut}}(p_{\ell^-} = z\tilde{p}_{\ell^-}, p_{\ell^+} = \tilde{p}_{\ell^+}, p_\gamma = (1-z)\tilde{p}_{\ell^-}) \right] + (p_{\ell^-} \leftrightarrow p_{\ell^+}), \end{aligned} \quad (3.5)$$

where  $\tilde{m}_{\ell\ell}^2 = (\tilde{p}_{\ell^-} + \tilde{p}_{\ell^+})^2$  is  $z$ -independent and the tilde over  $d\widetilde{\text{PS}}_3$  is to indicate that the integration is over the momenta  $\tilde{p}_{\ell^\pm}$ . The plus distribution is defined in the usual way,  $\int_0^1 [f(z)]_+ g(z) dz = \int_0^1 f(z)[g(z) - g(1)] dz$ , and the function  $\Theta_{\text{cut}}$  indicates which momenta are subject to phase space cuts. The functions  $G^{(\text{sub})}$  and  $\bar{\mathcal{G}}_{\text{MR}}$  are given by [43]

$$\begin{aligned} G^{(\text{sub})}(\tilde{m}_{\ell\ell}^2) &= \Gamma(1+\epsilon) \left( \frac{4\pi\mu^2}{\tilde{m}_{\ell\ell}^2} \right)^\epsilon \left( \frac{1}{\epsilon^2} + \frac{3}{2\epsilon} \right) + \frac{7}{2} - \frac{\pi^2}{3} \\ \bar{\mathcal{G}}_{\text{MR}}(\tilde{m}_{\ell\ell}^2, z) &= \hat{P}_{ff} \left[ \ln \left( \frac{\tilde{m}_{\ell\ell}^2}{m_\ell^2} \right) + \ln z - 1 \right] + (1+z) \ln(1-z) + 1 - z, \end{aligned} \quad (3.6)$$

where  $\hat{P}_{ff} = (1+z^2)/(1-z)$ . For inclusive observables, the contribution from  $\bar{\mathcal{G}}_{\text{MR}}$  vanishes and one recovers the massless limit of the subtraction described in Section 2.2. IR singularities from the virtual diagrams cancel with those in  $G^{(\text{sub})}$ , while the physical lepton mass  $m_\ell$  in  $\bar{\mathcal{G}}_{\text{MR}}$  acts as a regulator for the additional collinear singularities in non-inclusive observables.

Denoting by  $i$  the flavour index of the lepton  $\ell_i \in (e, \mu, \tau)$ , our result for the inclusive  $h \rightarrow Z\ell_i^+\ell_i^-$  partial width is given by (note that the index  $i$  is not summed over),

$$\begin{aligned} \Gamma_{\text{LO}}(h \rightarrow Z\ell_i^+\ell_i^-) &= 2.95 \times 10^{-6} \text{ GeV} \\ &+ \left( \frac{1 \text{ TeV}}{\Lambda} \right)^2 \left( -0.255C_{\phi B} + 0.358C_{\phi\square} + 0.0596C_{\phi D} + 0.0802C_{\phi W} \right. \\ &- 0.153C_{\phi WB} + 0.358C_{ll}[1221] - 0.0207C_{\phi e}[ii] + 0.0258C_{\phi l}^{(1)}[ii] - 0.358C_{\phi l}^{(3)}[11] \\ &\left. - 0.358C_{\phi l}^{(3)}[22] + 0.0258C_{\phi l}^{(3)}[ii] \right) \times 10^{-6} \text{ GeV} \end{aligned} \quad (3.7)$$

---

<sup>9</sup>A similar approach may be used to implement non-inclusive observables for other  $h \rightarrow Vf\bar{f}$  decays as well. However, these are less phenomenologically relevant and more susceptible to neglected resummation effects from parton showering. We leave this for future work.

$$\begin{aligned}
\delta\Gamma_{\text{NLO}}(h \rightarrow Z\ell_i^+\ell_i^-) &= 0.0416 \times 10^{-6} \text{ GeV} \\
&+ \left( \frac{1 \text{ TeV}}{\Lambda} \right)^2 \left( -0.00726C_\phi + 0.18C_{\phi B} + 0.0218C_{\phi\square} - 0.0344C_{\phi D} - 0.185C_{\phi W} \right. \\
&+ 0.0899C_{\phi WB} + 0.00287C_W - 0.00488C_{eu}[ii33] - 0.00789C_{ll}[1122] \\
&+ 0.0101C_{ll}[1221] - 0.00632C_{lq}^{(1)}[ii33] + 0.00595C_{lq}^{(3)}[ii33] + 0.00606C_{lu}[ii33] \\
&+ 0.00191C_{\phi e}[ii] - 0.00758C_{\phi l}^{(1)}[ii] - 0.0164C_{\phi l}^{(3)}[11] - 0.0164C_{\phi l}^{(3)}[22] \\
&- 0.00512C_{\phi l}^{(3)}[ii] + 0.017C_{\phi q}^{(1)}[33] - 0.00108C_{\phi q}^{(3)}[11] - 0.00108C_{\phi q}^{(3)}[22] \\
&- 0.0214C_{\phi q}^{(3)}[33] - 0.0191C_{\phi u}[33] + 0.00509C_{qe}[33ii] + 0.00243C_{u\phi}[33] \\
&\left. - 0.00655C_{uW}[33] \right) \times 10^{-6} \text{ GeV}, \tag{3.8}
\end{aligned}$$

where we have dropped contributions smaller than  $10^{-9}$  GeV in both  $\Gamma_{\text{LO}}$  and  $\delta\Gamma_{\text{NLO}}$ .

Results for differential distributions are given in Sec. 3.6.1. As pointed out in [26], care should be taken when applying these results to LHC studies, since the experimental cut on  $m_{\ell\ell}$  significantly impacts the results for some coefficients.

### 3.1.2 $h \rightarrow Z\nu\bar{\nu}$

The process  $h \rightarrow Z\nu\bar{\nu}$  is the simplest three-body decay since there are no charged particles in the final state. At this order, there are no IR divergences or real emission contributions to consider. We sum over final state neutrino flavours since they are unobservable, finding the result

$$\begin{aligned}
\Gamma_{\text{LO}}(h \rightarrow Z\nu\bar{\nu}) &= 17.5 \times 10^{-6} \text{ GeV} \\
&+ \left( \frac{1 \text{ TeV}}{\Lambda} \right)^2 \left( -0.231C_{\phi B} + 2.13C_{\phi\square} - 0.806C_{\phi W} - 0.433C_{\phi WB} \right. \\
&+ 2.12C_{ll}[1221] - 0.0464C_{\phi l}^{(1)}[11] - 0.0464C_{\phi l}^{(1)}[22] - 0.0464C_{\phi l}^{(1)}[33] \\
&- 2.08C_{\phi l}^{(3)}[11] - 2.08C_{\phi l}^{(3)}[22] + 0.0462C_{\phi l}^{(3)}[33] - 0.00114C_{\phi q}^{(3)}[11] \\
&\left. - 0.00114C_{\phi q}^{(3)}[22] \right) \times 10^{-6} \text{ GeV} \tag{3.9}
\end{aligned}$$

$$\begin{aligned}
\delta\Gamma_{\text{NLO}}(h \rightarrow Z\nu\bar{\nu}) &= 0.404 \times 10^{-6} \text{ GeV} \\
&+ \left( \frac{1 \text{ TeV}}{\Lambda} \right)^2 \left( -0.0431C_\phi - 0.0111C_{\phi B} + 0.148C_{\phi\square} + 0.0449C_{\phi D} \right. \\
&- 0.0209C_{\phi W} + 0.0172C_{\phi WB} + 0.00698C_W - 0.047C_{ll}[1122] \\
&+ 0.0881C_{ll}[1221] + 0.0114C_{lq}^{(1)}[1133] + 0.0114C_{lq}^{(1)}[2233] + 0.0114C_{lq}^{(1)}[3333] \\
&+ 0.0165C_{lq}^{(3)}[1133] + 0.0165C_{lq}^{(3)}[2233] + 0.0107C_{lq}^{(3)}[3333] - 0.0109C_{lu}[1133] \\
&- 0.0109C_{lu}[2233] - 0.0109C_{lu}[3333] + 0.012C_{\phi l}^{(1)}[11] + 0.012C_{\phi l}^{(1)}[22] \\
&+ 0.0142C_{\phi l}^{(1)}[33] - 0.136C_{\phi l}^{(3)}[11] - 0.136C_{\phi l}^{(3)}[22] - 0.0121C_{\phi l}^{(3)}[33] \\
&+ 0.0924C_{\phi q}^{(1)}[33] - 0.00719C_{\phi q}^{(3)}[11] - 0.00719C_{\phi q}^{(3)}[22] - 0.112C_{\phi q}^{(3)}[33] \\
&- 0.00138C_{\phi u}[11] - 0.00138C_{\phi u}[22] - 0.0964C_{\phi u}[33] - 0.00476C_{uB}[33] \\
&\left. + 0.015C_{u\phi}[33] + 0.00889C_{uW}[33] \right) \times 10^{-6} \text{ GeV}, \tag{3.10}
\end{aligned}$$

where we have dropped contributions smaller than  $10^{-9}$  GeV.

### 3.1.3 $h \rightarrow Zq\bar{q}$

The process  $h \rightarrow Zq\bar{q}$  is similar to  $Z\ell^+\ell^-$ , with the addition of QCD real and virtual corrections. We consider only inclusive observables since these are of primary interest, although non-inclusive observables may be computed by using fragmentation functions as described in [43].

At LO, the partial width for the  $h \rightarrow Zd_i\bar{d}_i$  process is the same for  $b\bar{b}$ ,  $d\bar{d}$ , and  $s\bar{s}$  with appropriate flavour index swapping. Denoting by  $i$  the flavour index of the down-type quark  $d_i \in (d, s, b)$ , we find a result of

$$\begin{aligned}
\Gamma_{\text{LO}}(h \rightarrow Zd_i\bar{d}_i) &= 13.1 \times 10^{-6} \text{ GeV} \\
&+ \left( \frac{1 \text{ TeV}}{\Lambda} \right)^2 \left( -1.58C_{\phi B} + 1.59C_{\phi\square} + 0.387C_{\phi D} + 0.801C_{\phi W} - 0.842C_{\phi WB} \right. \\
&+ 1.59C_{ll}[1221] - 0.0207C_{\phi d}[ii] - 1.59C_{\phi l}^{(3)}[11] - 1.59C_{\phi l}^{(3)}[22] + 0.118C_{\phi q}^{(1)}[ii] \\
&\left. + 0.118C_{\phi q}^{(3)}[ii] \right) \times 10^{-6} \text{ GeV}. \tag{3.11}
\end{aligned}$$

At NLO, the process  $h \rightarrow Zb\bar{b}$  is special since there are more top-quark contributions with

a diagonal CKM than for the light fermions. The  $h \rightarrow Zb\bar{b}$  result is given by

$$\begin{aligned}
\delta\Gamma_{\text{NLO}}(h \rightarrow Zb\bar{b}) &= 0.047 \times 10^{-6} \text{ GeV} \\
&+ \left( \frac{1 \text{ TeV}}{\Lambda} \right)^2 \left( -0.0322C_\phi - 0.0113C_{\phi B} + 0.0795C_{\phi\Box} + 0.0496C_{\phi D} \right. \\
&- 0.0742C_{\phi G} + 0.0261C_{\phi W} + 0.0934C_{\phi WB} + 0.00575C_W - 0.0349C_{ll}[1122] \\
&- 0.0103C_{ll}[1221] + 0.00381C_{lq}^{(3)}[1133] + 0.00381C_{lq}^{(3)}[2233] \\
&+ 0.00137C_{\phi d}[11] + 0.00137C_{\phi d}[22] + 0.00201C_{\phi d}[33] + 0.00137C_{\phi e}[11] \\
&+ 0.00137C_{\phi e}[22] + 0.00137C_{\phi e}[33] + 0.00137C_{\phi l}^{(1)}[33] - 0.0173C_{\phi l}^{(3)}[11] \\
&- 0.0175C_{\phi l}^{(3)}[22] - 0.0015C_{\phi l}^{(3)}[33] - 0.00137C_{\phi q}^{(1)}[11] - 0.00137C_{\phi q}^{(1)}[22] \\
&+ 0.0478C_{\phi q}^{(1)}[33] - 0.00451C_{\phi q}^{(3)}[11] - 0.00451C_{\phi q}^{(3)}[22] - 0.0779C_{\phi q}^{(3)}[33] \\
&- 0.00274C_{\phi u}[11] - 0.00274C_{\phi u}[22] - 0.0842C_{\phi u}[33] + 0.00524C_{qd}^{(1)}[3333] \\
&- 0.0587C_{qq}^{(1)}[3333] - 0.00311C_{qq}^{(3)}[1133] - 0.00311C_{qq}^{(3)}[2233] + 0.0195C_{qq}^{(3)}[3333] \\
&+ 0.0279C_{qu}^{(1)}[3333] + 0.00463C_{uB}[33] - 0.00488C_{ud}^{(1)}[3333] - 0.0055C_{u\phi}[33] \\
&\left. - 0.0452C_{uW}[33] \right) \times 10^{-6} \text{ GeV}. \tag{3.12}
\end{aligned}$$

For the  $h \rightarrow Zd\bar{d}$  and  $h \rightarrow Zs\bar{s}$  channels, we have

$$\begin{aligned}
\delta\Gamma_{\text{NLO}}(h \rightarrow Zd_i\bar{d}_i)_{d_i \neq b} &= 0.493 \times 10^{-6} \text{ GeV} \\
&+ \left( \frac{1 \text{ TeV}}{\Lambda} \right)^2 \left( -0.0322C_\phi - 0.0447C_{\phi B} + 0.134C_{\phi\Box} + 0.0625C_{\phi D} \right. \\
&- 0.0741C_{\phi G} + 0.00995C_{\phi W} + 0.0801C_{\phi WB} + 0.0162C_W - 0.0349C_{ll}[1122] \\
&+ 0.0709C_{ll}[1221] + 0.00432C_{lq}^{(3)}[1133] + 0.00432C_{lq}^{(3)}[2233] + 0.00064C_{\phi d}[ii] \\
&+ 0.00137C_{\phi d}[11] + 0.00137C_{\phi d}[22] + 0.00137C_{\phi d}[33] + 0.00137C_{\phi e}[11] \\
&+ 0.00137C_{\phi e}[22] + 0.00137C_{\phi e}[33] + 0.00137C_{\phi l}^{(1)}[33] - 0.0988C_{\phi l}^{(3)}[11] \\
&- 0.0988C_{\phi l}^{(3)}[22] - 0.0015C_{\phi l}^{(3)}[33] - 0.0293C_{\phi q}^{(1)}[ii] - 0.00137C_{\phi q}^{(1)}[11] \\
&- 0.00137C_{\phi q}^{(1)}[22] + 0.0782C_{\phi q}^{(1)}[33] - 0.0182C_{\phi q}^{(3)}[ii] - 0.00451C_{\phi q}^{(3)}[11] \\
&- 0.00451C_{\phi q}^{(3)}[22] - 0.1C_{\phi q}^{(3)}[33] - 0.00274C_{\phi u}[11] - 0.00274C_{\phi u}[22] \\
&- 0.0906C_{\phi u}[33] + 0.00509C_{qd}^{(1)}[33ii] - 0.0583C_{qq}^{(1)}[ii33] - 0.00281C_{qq}^{(3)}[iiii] \\
&- 0.00311C_{qq}^{(3)}[1122] + 0.0549C_{qq}^{(3)}[ii33] - 0.0354C_{qq}^{(3)}[i33i] + 0.0279C_{qu}^{(1)}[ii33] \\
&+ 0.00632C_{uB}[33] - 0.00488C_{ud}^{(1)}[3311] + 0.0105C_{u\phi}[33] \\
&\left. - 0.0456C_{uW}[33] \right) \times 10^{-6} \text{ GeV}. \tag{3.13}
\end{aligned}$$

The up-type channels have the LO and NLO results,

$$\begin{aligned}
\Gamma_{\text{LO}}(h \rightarrow Z u_i \bar{u}_i) &= 10.2 \times 10^{-6} \text{ GeV} \\
&+ \left( \frac{1 \text{ TeV}}{\Lambda} \right)^2 \left( -1.75 C_{\phi B} + 1.24 C_{\phi \square} + 0.446 C_{\phi D} + 1.15 C_{\phi W} \right. \\
&- 0.852 C_{\phi WB} + 1.24 C_{ll}[1221] - 1.24 C_{\phi l}^{(3)}[11] - 1.24 C_{\phi l}^{(3)}[22] \\
&\left. - 0.0981 C_{\phi q}^{(1)}[ii] + 0.0974 C_{\phi q}^{(3)}[ii] + 0.0413 C_{\phi u}[ii] \right) \times 10^{-6} \text{ GeV}
\end{aligned} \tag{3.14}$$

$$\begin{aligned}
\delta \Gamma_{\text{NLO}}(h \rightarrow Z u_i \bar{u}_i) &= 0.293 \times 10^{-6} \text{ GeV} \\
&+ \left( \frac{1 \text{ TeV}}{\Lambda} \right)^2 \left( -0.0251 C_{\phi} + 0.131 C_{\phi B} + 0.0931 C_{\phi \square} + 0.0158 C_{\phi D} \right. \\
&- 0.0578 C_{\phi G} - 0.154 C_{\phi W} + 0.164 C_{\phi WB} + 0.0167 C_W - 0.0272 C_{ll}[1122] \\
&+ 0.038 C_{ll}[1221] + 0.00337 C_{lq}^{(3)}[1133] + 0.00337 C_{lq}^{(3)}[2233] + 0.00139 C_{\phi d}[11] \\
&+ 0.00139 C_{\phi d}[22] + 0.00139 C_{\phi d}[33] + 0.00139 C_{\phi e}[11] + 0.00139 C_{\phi e}[22] \\
&+ 0.00139 C_{\phi e}[33] + 0.00139 C_{\phi l}^{(1)}[33] - 0.0596 C_{\phi l}^{(3)}[11] - 0.0596 C_{\phi l}^{(3)}[22] \\
&- 0.00106 C_{\phi l}^{(3)}[33] + 0.02449 C_{\phi q}^{(1)}[ii] - 0.00139 C_{\phi q}^{(1)}[11] - 0.00139 C_{\phi q}^{(1)}[22] \\
&+ 0.0643 C_{\phi q}^{(1)}[33] - 0.01401 C_{\phi q}^{(3)}[ii] - 0.00319 C_{\phi q}^{(3)}[11] - 0.00319 C_{\phi q}^{(3)}[22] \\
&- 0.0842 C_{\phi q}^{(3)}[33] - 0.00143 C_{\phi u}[ii] - 0.00277 C_{\phi u}[11] - 0.00277 C_{\phi u}[22] \\
&- 0.0776 C_{\phi u}[33] + 0.0481 C_{qq}^{(1)}[ii33] + 0.0144 C_{qq}^{(1)}[i33i] \\
&- 0.00213 C_{qq}^{(3)}[iiii] - 0.00256 C_{qq}^{(3)}[1122] + 0.0453 C_{qq}^{(3)}[ii33] + 0.0152 C_{qq}^{(3)}[i33i] \\
&- 0.0231 C_{qu}^{(1)}[ii33] - 0.0102 C_{qu}^{(1)}[33ii] + 0.00862 C_{uB}[33] \\
&+ 0.00794 C_{u\phi}[33] + 0.0195 C_{uu}[ii33] + 0.006 C_{uu}[i33i] \\
&\left. - 0.0552 C_{uW}[33] \right) \times 10^{-6} \text{ GeV},
\end{aligned} \tag{3.15}$$

where  $u_i \in (u, c)$  is the final state up-type quark flavour. In all these channels we have dropped contributions smaller than  $10^{-9}$  GeV in both  $\Gamma_{\text{LO}}$  and  $\delta \Gamma_{\text{NLO}}$ .

### 3.2 $h \rightarrow W f \bar{f}'$

Just as for  $h \rightarrow Z f \bar{f}$ , the SM corrections to  $h \rightarrow W f \bar{f}'$  are a subset of the full  $h \rightarrow 4f$  process, which are known to NLO EW and QCD in the SM [62–65]. The corrections most relevant for  $h \rightarrow W f \bar{f}'$  are implemented in PROPHECY4F [66] and HDECAY [67].

In the SMEFT, we compute for the first time the physical  $h \rightarrow W f \bar{f}'$  process at NLO, superseding the known (kinematically unphysical)  $h \rightarrow WW^*$  results [23]. In our numerical results we have summed over  $h \rightarrow W^+ f \bar{f}'$  and the charge conjugate process  $h \rightarrow W^- f' \bar{f}$ .

Since the  $W$  is charged, real photon emission from the  $W$  makes massive dipole subtraction necessary, as described in Sec. 2.2. The structure of the QED IR poles for  $h \rightarrow W f \bar{f}'$  is

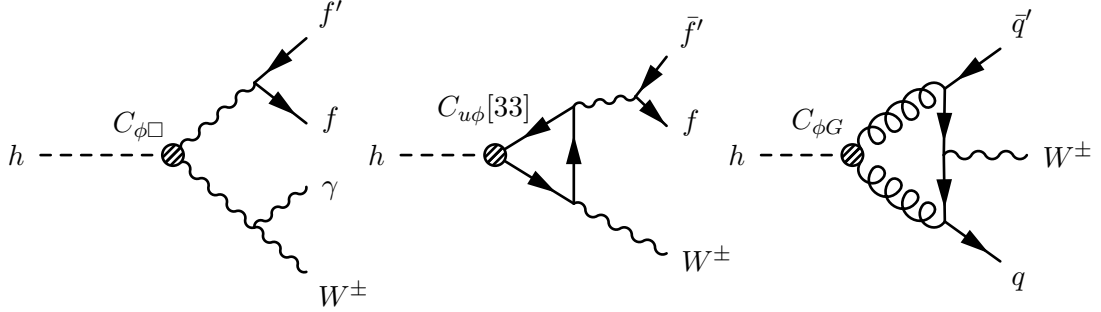


**Figure 2.** Representative diagrams for the  $h \rightarrow f\bar{f}'W^\pm$  decay process in the SMEFT. Dashed blobs represent SMEFT operator insertions.

the same as for  $q\bar{q} \rightarrow Wj$  [68], with appropriate swapping of initial and final state legs. We use the expressions for all dipole functions and phase space mappings given in [54] for the  $W$  as the emitter or spectator, and use the massless formulas given in [43] for the QCD and QED pairing of the fermion legs since we consider only the top quark to be massive.

### 3.2.1 $h \rightarrow W^\pm \ell^\mp \nu$

We first consider the simpler leptonic process  $h \rightarrow W^\pm \ell_i^\mp \nu_i$ , where  $\ell_i = (e, \mu, \tau)$ . There are no QCD corrections to this process at one-loop, and the QED dipole subtraction has only two terms, with the  $W$  and  $\ell$  each as emitter/spectator. We find at LO (summing over  $W^\pm$ , but not over  $i$ ),

$$\begin{aligned} \Gamma_{\text{LO}}(h \rightarrow W^\pm \ell_i^\mp \nu_i) &= 87.7 \times 10^{-6} \text{ GeV} \\ &+ \left( \frac{1 \text{ TeV}}{\Lambda} \right)^2 \left( 10.6 C_{\phi\Box} - 2.66 C_{\phi D} - 7.92 C_{\phi W} + 10.6 C_{ll}[1221] \right. \\ &- 10.6 C_{\phi l}^{(3)}[11] - 10.6 C_{\phi l}^{(3)}[22] + 1.63 C_{\phi l}^{(3)}[ii] - 0.00693 C_{\phi q}^{(3)}[11] \\ &\left. - 0.00693 C_{\phi q}^{(3)}[22] \right) \times 10^{-6} \text{ GeV}, \end{aligned} \quad (3.16)$$

where only the coefficient  $C_{\phi l}^{(3)}[ii]$  depends on the lepton flavour  $i$ . Here we have truncated coefficients arising from the width expansion that contribute less than  $10^{-9}$  GeV.

At NLO, we find

$$\begin{aligned}
\delta\Gamma_{\text{NLO}}(h \rightarrow W^\pm \ell_i^\mp \nu) = & 2.99 \times 10^{-6} \text{ GeV} \\
& + \left( \frac{1 \text{ TeV}}{\Lambda} \right)^2 \left( -0.173C_\phi - 0.0291C_{\phi B} + 0.834C_{\phi \square} - 0.334C_{\phi D} - 0.392C_{\phi W} \right. \\
& - 0.284C_{\phi WB} + 0.0283C_W + 0.385C_{ll}[1221] - 0.00477C_{ll}[1ii1] \\
& - 0.00477C_{ll}[2ii2] - 0.00477C_{ll}[3ii3] + 0.029C_{lq}^{(3)}[1133] + 0.029C_{lq}^{(3)}[2233] \\
& - 0.0187C_{lq}^{(3)}[ii11] - 0.0187C_{lq}^{(3)}[ii22] + 0.15C_{lq}^{(3)}[ii33] - 0.0109C_{\phi l}^{(1)}[11] \\
& - 0.0109C_{\phi l}^{(1)}[22] + 0.00362C_{\phi l}^{(1)}[ii] - 0.811C_{\phi l}^{(3)}[11] - 0.811C_{\phi l}^{(3)}[22] \\
& - 0.0604C_{\phi l}^{(3)}[ii] - 0.0448C_{\phi q}^{(3)}[11] - 0.0448C_{\phi q}^{(3)}[22] - 0.445C_{\phi q}^{(3)}[33] \\
& \left. - 0.0291C_{u\phi}[33] + 0.118C_{uW}[33] \right) \times 10^{-6} \text{ GeV} , \tag{3.17}
\end{aligned}$$

where we have not truncated any coefficients, and only  $C_{ll}$ ,  $C_{lq}^{(3)}$ ,  $C_{\phi l}^{(1)}$ , and  $C_{\phi l}^{(3)}$  have coefficients that depend on the final state lepton flavour  $i$ .

### 3.2.2 $h \rightarrow W^\pm q\bar{q}'$

We now move on to the hadronic process  $h \rightarrow W^\pm q_i\bar{q}'_i$ , where  $q_i\bar{q}'_i = (ud, cs)$ . Since we have final state quarks we must consider QCD corrections as well. The QCD dipole subtraction is identical to the  $h \rightarrow Zq\bar{q}$  case, whereas the QED dipole subtraction consists of six terms – two for each emitter/spectator pair among  $W^\pm q\bar{q}'$ . Summing over  $W^\pm$  but not over the flavour index  $i$ , we find the result

$$\begin{aligned}
\delta\Gamma_{\text{LO}}(h \rightarrow W^\pm q_i\bar{q}'_i) = & 263 \times 10^{-6} \text{ GeV} \\
& + \left( \frac{1 \text{ TeV}}{\Lambda} \right)^2 \left( 31.9C_{\phi \square} - 7.97C_{\phi D} - 23.8C_{\phi W} + 31.9C_{ll}[1221] \right. \\
& - 31.9C_{\phi l}^{(3)}[11] - 31.9C_{\phi l}^{(3)}[22] + 4.88C_{\phi q}^{(3)}[ii] - 0.0208C_{\phi q}^{(3)}[11] \\
& \left. - 0.0208C_{\phi q}^{(3)}[22] - 0.00693C_{\phi l}^{(3)}[33] \right) \times 10^{-6} \text{ GeV} , \tag{3.18}
\end{aligned}$$

where we have once again truncated coefficients coming from the expansion of  $\Gamma_W$  that contribute less than  $10^{-9}$  GeV.

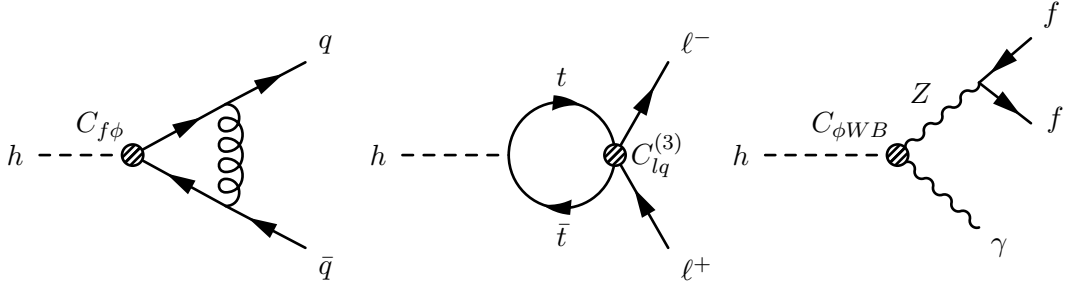


**Figure 3.** Representative diagrams for the  $h \rightarrow f\bar{f}$  decay process in the SMEFT at NLO. The dashed blobs represent SMEFT operator insertions.

At NLO, we find a correction

$$\begin{aligned}
 \delta\Gamma_{\text{NLO}}(h \rightarrow W^\pm q_i \bar{q}'_i) = & 18.8 \times 10^{-6} \text{ GeV} \\
 & + \left( \frac{1 \text{ TeV}}{\Lambda} \right)^2 \left( -0.519C_\phi - 0.0728C_{\phi B} + 3.7C_{\phi\square} - 1.3C_{\phi D} \right. \\
 & - 1.34C_{\phi G} - 4.48C_{\phi W} - 0.839C_{\phi WB} + 0.0848C_W + 2.35C_{ll}[1221] \\
 & - 0.0187C_{lq}^{(3)}[11ii] + 0.0869C_{lq}^{(3)}[1133] - 0.0187C_{lq}^{(3)}[22ii] + 0.0869C_{lq}^{(3)}[2233] \\
 & - 0.0187C_{lq}^{(3)}[33ii] - 0.0326C_{\phi l}^{(1)}[11] - 0.0326C_{\phi l}^{(1)}[22] - 3.63C_{\phi l}^{(3)}[11] \\
 & - 3.63C_{\phi l}^{(3)}[22] - 0.0448C_{\phi l}^{(3)}[33] - 0.00357C_{\phi q}^{(1)}[ii] + 0.0467C_{\phi q}^{(3)}[ii] \\
 & - 0.134C_{\phi q}^{(3)}[11] - 0.134C_{\phi q}^{(3)}[22] - 1.33C_{\phi q}^{(3)}[33] - 0.0143C_{qq}^{(1)}[iiii] \\
 & - 0.0143C_{qq}^{(1)}[1221] + 0.124C_{qq}^{(1)}[i33i] - 0.0979C_{qq}^{(3)}[iiii] \\
 & - 0.112C_{qq}^{(3)}[1122] + 0.901C_{qq}^{(3)}[ii33] + 0.0143C_{qq}^{(3)}[1221] \\
 & \left. - 0.124C_{qq}^{(3)}[i33i] - 0.0872C_{u\phi}[33] + 0.354C_{uW}[33] \right) \times 10^{-6} \text{ GeV}. \tag{3.19}
 \end{aligned}$$

### 3.3 $h \rightarrow f\bar{f}$

The Higgs decays to  $f\bar{f}$  are the most important branching ratios, constituting nearly 70% of the total Higgs width in the SM. The decays  $h \rightarrow b\bar{b}, c\bar{c}$  are known exactly at NNLO QCD in the SM [69–73], with further results available in various approximations [74–77]. The state of the art EW corrections in the SM [78–82] for  $h \rightarrow f\bar{f}$  are one-loop exact and known at two-loops in the  $m_t \rightarrow \infty$  expansion, as well two-loop mixed QCD-EW order [83]. The most numerically relevant corrections are implemented in MADGRAPH [84] and HDECAY [67].

In the SMEFT, all relevant  $h \rightarrow f\bar{f}$  decays are known at NLO in the dimension-6 SMEFT [18–20]. We have implemented an independent calculation for all  $f \in (b, c, s, \tau, \mu)$ . For the  $h \rightarrow f\bar{f}$  processes, we must keep the fermion mass  $m_f$  nonzero to have a non-vanishing

SM contribution. The LO widths are particularly simple since they are two-body decays:

$$\Gamma_{\text{LO}}(h \rightarrow f_i \bar{f}_i) = \frac{\sqrt{m_h^2 - 4m_{f_i}^2}}{16\pi m_h^2} |\mathcal{A}^{(0)}(h \rightarrow f_i \bar{f}_i)|^2 \quad (3.20)$$

where the amplitude squared to linear order in the dimension-6 SMEFT coefficients is given by (omitting the colour sum for quarks)

$$|\mathcal{A}^{(0)}(h \rightarrow f_i \bar{f}_i)|^2 = |\mathcal{A}_{\text{SM}}^{(0)}|^2 + \frac{2}{\Lambda^2} \text{Re}(\mathcal{A}_{\text{SM}}^{(0)*} \mathcal{A}_{\text{EFT}}^{(0)}) , \quad (3.21)$$

$$|\mathcal{A}_{\text{SM}}^{(0)}|^2 = 2\sqrt{2}G_\mu m_{f_i}^2(m_h^2 - 4m_{f_i}^2) , \quad (3.22)$$

$$\begin{aligned} \frac{2}{\Lambda^2} \text{Re}(\mathcal{A}_{\text{SM}}^{(0)*} \mathcal{A}_{\text{EFT}}^{(0)}) = & \frac{m_{f_i}^2(m_h^2 - 4m_{f_i}^2)}{\Lambda^2} \left[ -\frac{2^{5/4}}{m_{f_i} \sqrt{G_\mu}} C_{f\phi}[ii] \right. \\ & \left. + 4C_{\phi\Box} - C_{\phi D} - 2C_{\phi l}^{(3)}[11] - 2C_{\phi l}^{(3)}[22] + 2C_{ll}[1221] \right] . \end{aligned} \quad (3.23)$$

At NLO, each  $h \rightarrow f_i \bar{f}_i$  process must be considered separately. Representative diagrams at NLO for these processes are shown in Fig. 3. For each process, we include the effects of nonzero  $m_t, m_b, m_\tau$ , as well as all masses greater than or equal to  $m_{f_i}$  for consistency. We perform on-shell renormalization for all fermion masses, and discuss the effects of  $\overline{\text{MS}}$  masses at the end of this section. Since we consider  $m_{f_i} \neq 0$ , we use the massive dipole subtraction procedure discussed in Sec. 2.2 to handle IR singularities. As a cross check, we have also verified our subtraction procedure with a phase space slicing method [43] for these processes.

Since the  $Z$  and  $W$  do not appear as external states in this process, we consistently include their widths by using the complex mass scheme. Including the width is important to regulate a divergence in the real emission contribution to  $C_{\phi WB}$ ,  $C_{\phi B}$ , and  $C_{\phi W}$  through the third diagram depicted in Fig. 3 when the  $Z$  goes on-shell.

We consider the two leptonic final states  $\tau^+ \tau^-$  and  $\mu^+ \mu^-$ . We do not consider the  $e^+ e^-$  channel since the electron mass suppresses the  $h \rightarrow e^+ e^-$  rate to be unobservably small. For  $h \rightarrow \tau^+ \tau^-$ , we keep  $m_t, m_b$ , and  $m_\tau$  nonzero, while taking all lighter fermions massless. For  $h \rightarrow \mu^+ \mu^-$ , we take all of  $m_t, m_b, m_\tau, m_c$ , and  $m_\mu$  to be nonzero, while taking lighter fermions massless.

We consider three hadronic final states:  $b\bar{b}$ ,  $c\bar{c}$ , and  $s\bar{s}$ . The calculation is very similar to  $\ell^+ \ell^-$ , with the addition of virtual and real emission QCD contributions. For  $h \rightarrow b\bar{b}$ , we take nonzero  $m_t, m_b$ , and  $m_\tau$ . For  $h \rightarrow c\bar{c}$ , we take nonzero  $m_t, m_b, m_\tau$ , and  $m_c$ . Finally, we include results for  $h \rightarrow s\bar{s}$  for completeness, taking nonzero  $m_t, m_b, m_\tau, m_c, m_\mu$ , and  $m_s$ .

### 3.3.1 $\overline{\text{MS}}$ masses in $h \rightarrow q\bar{q}$

For the channels  $h \rightarrow q\bar{q}$ , it is well known that the choice of renormalization scheme for the quark masses  $m_b$ ,  $m_c$ , and  $m_s$  can make a significant numerical difference [57]. Therefore, while our results are mainly obtained in terms of OS SM parameters, we have considered also the  $\overline{\text{MS}}$  scheme for the light quark masses. The work in Ref. [20] and subsequent papers have a quite in-depth discussion on the relation between the two schemes for  $h \rightarrow q\bar{q}$  in the SMEFT. Here we summarize the main results presented in those papers, and refer to the original publications for more details.

In general, the relation between OS and  $\overline{\text{MS}}$  masses can be written as [85, 86]

$$m_q = m_q(\mu)(1 - \delta_q(\mu)), \quad (3.24)$$

where  $m_q$  and  $m_q(\mu)$  are the masses of a generic quark in the OS  $\overline{\text{MS}}$  and schemes, respectively. The function  $\delta_q(\mu)$  in general depends on the  $\overline{\text{MS}}$  mass of the quark, although one can use the OS mass instead, as the difference is of higher order. To obtain the relation between the Higgs width calculated in the two schemes

$$\Gamma_{\overline{\text{MS}}}(h \rightarrow q\bar{q}) = \Gamma_{\text{OS}}(h \rightarrow q\bar{q}) + \Delta\Gamma(h \rightarrow q\bar{q}) \quad (3.25)$$

it is sufficient to replace the OS mass with its expression in terms of the  $\overline{\text{MS}}$  mass and then expand to linear order in  $\delta_q(\mu)$ .

Finally, as the input values for the  $\overline{\text{MS}}$  quark masses are usually defined at or around the mass scale, we must evolve them to the scale  $\mu = m_h$  before obtaining the final result for the partial widths. This evolution depends on SMEFT coefficients, and so requires an implementation of the RGEs between  $m_q$  and  $\mu$ . This is beyond the current scope of NEWiSH, and so we cannot implement these in full generality. However, since this evolution is numerically important for these processes, we have evolved the Wilson coefficients appearing in  $\delta_q(\mu)$  by using DSIXTOOLS [87, 88] and the SM input masses with four-loop beta functions in RUNDEC [85, 86], and hard-coded the result for the specific inputs defined in Sec. 2.3. Numerical results using these inputs are also in App. B.

### 3.4 $h \rightarrow VV'$

The processes  $h \rightarrow VV'$  with  $VV' \in (gg, \gamma\gamma, Z\gamma)$  are unique since they first occur at the one-loop level in the SM, but have tree-level contributions in the SMEFT. Representative diagrams are shown in Fig. 4.

For our implementation of these processes, we only include dimension-6, one-loop accurate results<sup>10</sup>. To be explicit, the virtual amplitude for  $h \rightarrow VV'$  in the SMEFT is given by

$$\mathcal{A}_{VV'} = \frac{1}{\Lambda^2} \mathcal{A}_{\text{EFT}}^{(0)} + \frac{1}{(4\pi)^2} \mathcal{A}_{\text{SM}}^{(1)} + \frac{1}{(4\pi\Lambda)^2} \mathcal{A}_{\text{EFT}}^{(1)} + \dots \quad (3.26)$$

<sup>10</sup>The numerical effects of the partial higher order terms included in [27, 28] are generally small, so we leave their implementation in NEWiSH to future work.

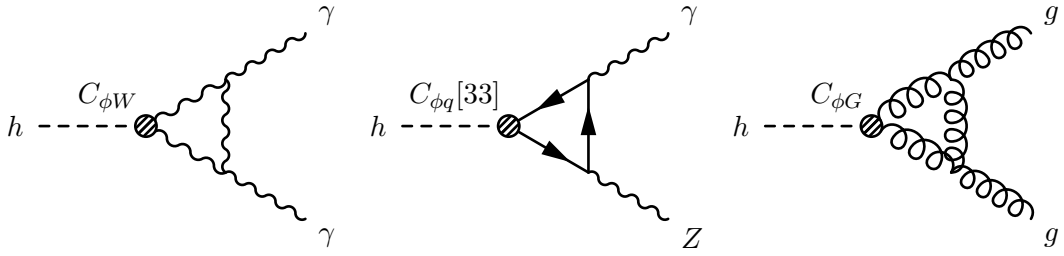


**Figure 4.** Representative diagrams for the  $h \rightarrow VV'$  decay processes in the SMEFT at NLO. Dashed blobs represent SMEFT operator insertions.

We define LO and NLO widths given by

$$\Gamma_{\text{LO}}(h \rightarrow VV') = \frac{c_{VV'}}{16\pi m_h} \left[ \frac{2}{(4\pi\Lambda)^2} \text{Re} \left( \mathcal{A}_{\text{EFT}}^{(0)*} \mathcal{A}_{\text{SM}}^{(1)} \right) \right], \quad (3.27)$$

$$\delta\Gamma_{\text{Virt}}(h \rightarrow VV') = \frac{c_{VV'}}{16\pi m_h} \left[ \frac{1}{(4\pi)^4} |\mathcal{A}_{\text{SM}}^{(1)}|^2 + \frac{2}{(4\pi)^4 \Lambda^2} \text{Re} \left( \mathcal{A}_{\text{EFT}}^{(1)*} \mathcal{A}_{\text{SM}}^{(1)} \right) \right], \quad (3.28)$$

where the prefactor  $c_{VV'}$  is equal to  $1 - M_Z^2/m_h^2$  for  $h \rightarrow Z\gamma$  and 1 for  $h \rightarrow (\gamma\gamma, gg)$ . We include a nonzero  $m_b$  in the SM virtual amplitudes, but other light quarks are considered massless. For  $h \rightarrow \gamma\gamma, Z\gamma$ , there are no real emission contributions so this is the full result up to one-loop order and  $\Gamma_{\text{NLO}} \equiv \Gamma_{\text{LO}} + \delta\Gamma_{\text{Virt}}$ .

In the SM, the state of the art for  $h \rightarrow \gamma\gamma$  is NLO EW (two-loop) [82, 89–91], full NNLO (three-loop) QCD [92, 93], and N<sup>3</sup>LO QCD [94] in the  $m_t \rightarrow \infty$  limit. The  $h \rightarrow Z\gamma$  process is known in the SM at NLO EW [95, 96] and NLO QCD [97–99], which are both two-loop order. In the SMEFT,  $h \rightarrow \gamma\gamma$  has been calculated in [23–25] at one-loop using both the  $(M_W, M_Z, G_\mu)$  and  $(\alpha, M_Z, G_\mu)$  input schemes. The  $h \rightarrow Z\gamma$  process is likewise known at one-loop [21, 22].

The SM result for  $h \rightarrow gg$  is a component of the full  $h \rightarrow$  hadrons process, which is known to approximate N<sup>4</sup>LO QCD [74, 76] (see also [4–6] for a more complete discussion).

For  $h \rightarrow gg$ , there is in addition to the virtual correction of Eq. (3.28), a real emission contribution proportional to  $C_{\phi G}$  from  $h \rightarrow \Sigma_i f_i \bar{f}_i g$  and  $h \rightarrow ggg$ . These contributions are trivially found from the  $h \rightarrow gg$  NLO SM calculation in the  $m_t \rightarrow \infty$  limit [6]. We note that in the NLO SMEFT, the SM contribution occurs through the one-loop triangle graph and SM corrections to this diagram are higher order. To include higher order SM corrections consistently, the two-loop contributions proportional to  $C_{\phi G}$  would be needed, along with one-loop real contributions [60].

For operators other than  $C_{\phi G}$ , the contributions to  $h \rightarrow gg$  first arise at one-loop and can be included to  $\mathcal{O}(\frac{1}{16\pi^2 \Lambda^4})$ . In order to keep the power counting consistent, we have chosen not to include these terms as they are numerically small [61]. In addition, the decay  $h \rightarrow gg$  has been calculated to all orders in  $\frac{v^2}{\Lambda^2}$  using geoSMEFT [27, 28].

We present numerical results for  $h \rightarrow VV'$ ,  $VV' \in (\gamma\gamma, Z\gamma, gg)$  in App. B.3.

### 3.5 $h \rightarrow ggZ$

The process  $h \rightarrow ggZ$  is a rare loop-induced decay in the SM [59, 100, 101], with a very small rate. In the SMEFT, it may be determined from the calculation of  $gg \rightarrow Z h$ , which is known at NLO in the SMEFT [102]. The process can be written as

$$g_\mu^a(p_1) g_\nu^b(p_2) \rightarrow h(-p_3) Z(-p_4), \quad (3.29)$$

The Feynman amplitudes for these decay scatterings are given by

$$\mathcal{A}_{hZ} = i\sqrt{2} \frac{M_Z G_\mu \alpha_S(\mu_R)}{\pi} \delta_{ab} \epsilon_\mu^a(p_1) \epsilon_\nu^b(p_2) \epsilon_\rho^*(p_3) \hat{\mathcal{A}}_{hZ}^{\mu\nu\rho}(p_1, p_2, p_3) \quad (3.30)$$

where  $\epsilon(p_i)$  is the polarisation vector of the  $i_{th}$  particle,  $G_\mu$  is the Fermi constant and  $\alpha_S$  is the QCD fine structure constant defined at the renormalization scale  $\mu_R$ . For  $hZ$  production we have:

$$\mathcal{A}_{hZ}^{\mu\nu\rho} = \sum_i^7 \mathcal{P}_i^{\mu\nu\rho} A_{ihZ}, \quad (3.31)$$

where  $\mathcal{P}_i$  are a basis of orthonormal projectors and  $A_{ihZ}$  are the associated scalar form factors [103]. These latter depend only on scalar quantities, namely the top quark mass  $m_t$ , the masses of the external particles and the partonic Mandelstam variables.

Since the process is loop-induced in both the SM and the SMEFT, the partial width is negligibly small, though the momentum swapped process  $gg \rightarrow Z h$  is important at the LHC [102]. For completeness, we find explicitly:

$$\begin{aligned} \Gamma_{\text{NLO}}(h \rightarrow ggZ) &= 2.26 \times 10^{-9} \text{ GeV} \\ &+ \left( \frac{1 \text{ TeV}}{\Lambda} \right)^2 \left( 0.274 C_{\phi\Box} + 0.00711 C_{\phi G} + 0.274 C_{ll}[1221] \right. \\ &\quad \left. - 0.274 C_{\phi l}^{(3)}[11] - 0.274 C_{\phi l}^{(3)}[22] + 0.0365 C_{uG}[33] \right) \times 10^{-9} \text{ GeV}, \end{aligned} \quad (3.32)$$

where we have dropped contributions smaller than  $10^{-11}$  GeV, and there are no tree-level or real emission contributions.

### 3.6 $h \rightarrow 4f$ and the narrow width approximation

Thanks to our implementation of  $h \rightarrow f\bar{f}V$ , we have access to the  $h \rightarrow 4f$  processes at NLO through the narrow width approximation (NWA). At LO, the full results are known and have been studied in [42]. We use the complex mass scheme at LO for the  $4f$  process and neglect the  $W$  and  $Z$  widths in the NLO  $h \rightarrow f_1\bar{f}_2V$  corrections which are combined with the NLO  $V \rightarrow f_3\bar{f}_4$  contributions using the NWA.

For the total  $h \rightarrow 4f$  prediction, a subtlety appears in the treatment of the  $W$  and  $Z$  widths. In the usual approach of the complex mass scheme, one takes the experimental values for

$(\Gamma_W, \Gamma_Z)$  as inputs. However, since a number of SMEFT operators contribute to  $\Gamma_V$ , it is more appropriate to express  $\Gamma_V$  using our other input parameters and expand it in powers of  $\Lambda$ . This is the approach adopted in [42]<sup>11</sup> and gives a narrow width approximation,

$$\begin{aligned} \Gamma_{\text{NWA}}(h \rightarrow 4f) &= \Gamma(h \rightarrow f\bar{f}V) \times \frac{\Gamma(V \rightarrow f\bar{f})}{\Gamma(V \rightarrow \text{all})} \\ &= \Gamma_{\text{SM}, \text{NWA}} + \frac{1}{\Lambda^2} \left[ \Gamma_{\text{EFT}}^{(0)}(f\bar{f}V) \times \text{BR}_{\text{SM}}^{(0)}(V \rightarrow f\bar{f}) + \Gamma_{\text{SM}}^{(0)}(f\bar{f}V) \times \text{BR}_{\text{EFT}}^{(0)}(V \rightarrow f\bar{f}) \right] \\ &+ \frac{1}{16\pi^2\Lambda^2} \left[ \Gamma_{\text{EFT}}^{(1)}(f\bar{f}V) \times \text{BR}_{\text{SM}}^{(0)}(V \rightarrow f\bar{f}) + \Gamma_{\text{SM}}^{(0)}(f\bar{f}V) \times \text{BR}_{\text{EFT}}^{(1)}(V \rightarrow f\bar{f}) \right. \\ &\quad \left. + \Gamma_{\text{EFT}}^{(0)}(f\bar{f}V) \times \text{BR}_{\text{SM}}^{(1)}(V \rightarrow f\bar{f}) + \Gamma_{\text{SM}}^{(1)}(f\bar{f}V) \times \text{BR}_{\text{EFT}}^{(0)}(V \rightarrow f\bar{f}) \right], \end{aligned} \quad (3.33)$$

where the superscript is the loop order, and the branching ratios are expanded in loop orders and powers of  $\Lambda$ . Writing  $(V \rightarrow f\bar{f})$  and  $(V \rightarrow \text{all})$  as  $(f\bar{f})$  and  $(\text{all})$  for brevity, we have explicitly

$$\begin{aligned} \text{BR}_{\text{SM}}(V \rightarrow f\bar{f}) &= \frac{\Gamma_{\text{SM}}(f\bar{f})}{\Gamma_{\text{SM}}(\text{all})} \\ &= \frac{\Gamma_{\text{SM}}^{(0)}(f\bar{f})}{\Gamma_{\text{SM}}^{(0)}(\text{all})} + \frac{1}{16\pi^2} \left[ \frac{\Gamma_{\text{SM}}^{(1)}(f\bar{f})}{\Gamma_{\text{SM}}^{(0)}(\text{all})} - \frac{\Gamma_{\text{SM}}^{(0)}(f\bar{f}) \times \Gamma_{\text{SM}}^{(1)}(\text{all})}{\left[ \Gamma_{\text{SM}}^{(0)}(\text{all}) \right]^2} \right] \\ &= \text{BR}_{\text{SM}}^{(0)}(f\bar{f}) + \frac{1}{16\pi^2} \text{BR}_{\text{SM}}^{(1)}(f\bar{f}), \end{aligned} \quad (3.34)$$

$$\begin{aligned} \text{BR}_{\text{EFT}}(V \rightarrow f\bar{f}) &= \frac{1}{\Lambda^2} \text{BR}_{\text{EFT}}^{(0)}(f\bar{f}) + \frac{1}{16\pi^2\Lambda^2} \text{BR}_{\text{EFT}}^{(1)}(f\bar{f}) \\ &= \frac{1}{\Lambda^2} \left[ \frac{\Gamma_{\text{EFT}}^{(0)}(f\bar{f})}{\Gamma_{\text{SM}}^{(0)}(\text{all})} - \text{BR}_{\text{SM}}^{(0)}(f\bar{f}) \frac{\Gamma_{\text{EFT}}^{(0)}(\text{all})}{\Gamma_{\text{SM}}^{(0)}(\text{all})} \right] \\ &+ \frac{1}{16\pi^2\Lambda^2} \left[ \frac{\Gamma_{\text{EFT}}^{(1)}(f\bar{f})}{\Gamma_{\text{SM}}^{(0)}(\text{all})} - \text{BR}_{\text{SM}}^{(0)}(f\bar{f}) \frac{\Gamma_{\text{EFT}}^{(1)}(\text{all})}{\Gamma_{\text{SM}}^{(0)}(\text{all})} - \text{BR}_{\text{SM}}^{(1)}(f\bar{f}) \frac{\Gamma_{\text{EFT}}^{(0)}(\text{all})}{\Gamma_{\text{SM}}^{(0)}(\text{all})} \right. \\ &\quad \left. + 2\text{BR}_{\text{SM}}^{(0)}(f\bar{f}) \frac{\Gamma_{\text{EFT}}^{(0)}(\text{all}) \Gamma_{\text{SM}}^{(1)}(\text{all})}{\left[ \Gamma_{\text{SM}}^{(0)}(\text{all}) \right]^2} - \frac{\Gamma_{\text{EFT}}^{(0)}(f\bar{f}) \Gamma_{\text{SM}}^{(1)}(\text{all})}{\left[ \Gamma_{\text{SM}}^{(0)}(\text{all}) \right]^2} \right]. \end{aligned} \quad (3.35)$$

To implement this at LO without the NWA, we must write the widths  $\Gamma_V$  in terms of  $\Lambda$  and expand the total amplitude squared again:

$$\begin{aligned} |\mathcal{A}(h \rightarrow 4f)|^2 &= |\mathcal{A}_{\text{SM}}|^2 + \frac{2}{\Lambda^2} \text{Re} \left( \mathcal{A}_{\text{SM}}^{(0)*} \times \mathcal{A}_{\text{EFT}}^{(0)} \right) \Big|_{\Gamma_V = \Gamma_{\text{SM}}^{(0)}(V \rightarrow \text{all})} \\ &+ \frac{\Gamma_{\text{EFT}}^{(0)}(V \rightarrow \text{all})}{\Lambda^2} \left( \frac{\partial}{\partial \Gamma_V} |\mathcal{A}_{\text{SM}}|^2 \right) \Big|_{\Gamma_V = \Gamma_{\text{SM}}^{(0)}(V \rightarrow \text{all})}. \end{aligned} \quad (3.36)$$

<sup>11</sup>We have verified that we have reasonable agreement with [42] at LO.

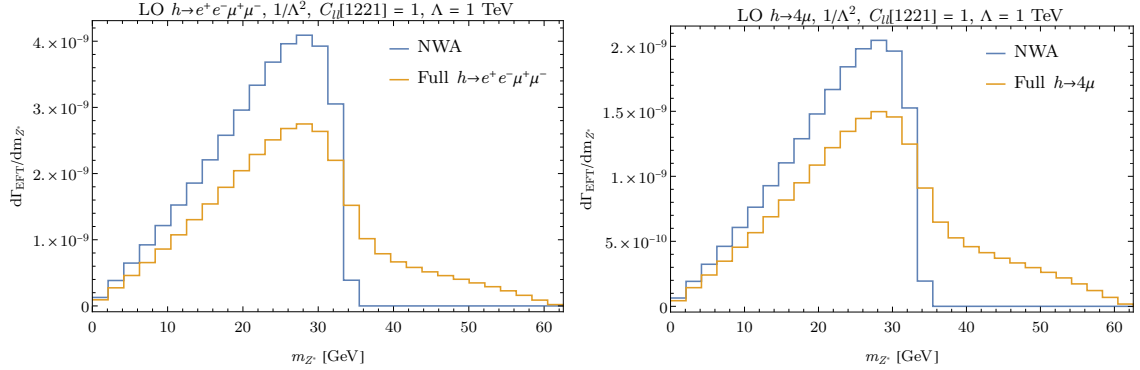


**Figure 5.** A comparison of the narrow width approximation and full  $h \rightarrow 4\ell$  results for  $C_{ll}[1221]$ , where the narrow width approximation works similarly for both  $e^+e^-\mu^+\mu^-$  (left) and  $4\mu$  (right) channels. Here  $m_{Z^*}$  is defined to be the invariant mass of the opposite pair of same flavour opposite sign leptons from the pair with invariant mass closest to  $M_Z$ .

It is important to estimate how well the NWA approximates the full results. We can do this comparison only at LO, which should give a rough idea for what to expect at NLO. For specific subprocesses, such as  $h \rightarrow 4\mu$ , it can fail badly for specific coefficients, as shown in the next subsection. However, for most operators and individual  $h \rightarrow f_1\bar{f}_2f_3\bar{f}_4$  subprocesses, the agreement is at the  $\sim 10\%$  level. In the total  $h \rightarrow 4f$  width, this remains true for bosonic operators and those entering  $X_H$ . For fermionic operators, on the other hand, a delicate cancellation occurs between channels that results in the NWA and full result disagreeing at an  $\mathcal{O}(1)$  level. This can be seen from Table 9 of [42], and is a manifestation of the fact that the sum of partial widths equals the total width, i.e.  $\sum_X \Gamma(h \rightarrow X)/\Gamma_V = 1$ . In the total  $4f$  width, this cancellation is exact in the NWA, whereas in the full result off-shell and interference effects violate it.

### 3.6.1 Differential distributions for $h \rightarrow 4\ell$

As discussed in Sec. 3.1.1, we have implemented differential distributions in the dilepton invariant mass distributions,  $d\Gamma/dm_{\ell\ell}$ , for the  $h \rightarrow 4\ell$  channel since they are especially relevant at the LHC. These distributions are also particularly useful for analysing the validity of the NWA and how it fails.

To make a connection to the three-body  $h \rightarrow \ell^+\ell^-Z$  process, we define  $m_Z^{\ell\ell}$  to be the opposite sign, same flavour dilepton invariant mass closest to  $m_Z^{\ell\ell}$ , and  $m_{Z^*}$  to be the opposite pair. For example, for  $h \rightarrow e^+(p_1)e^-(p_2)\mu^+(p_3)\mu^-(p_4)$ ,  $m_Z^{\ell\ell} = \max(m_{12}, m_{34})$  and  $m_{Z^*} = \min(m_{12}, m_{34})$ . For the  $4\mu$  and  $4e$  channels, one must also consider  $m_{14}$  and  $m_{23}$ .

We show results for two select coefficients in Figs. 5 and 6 at LO for both the  $e^+e^-\mu^+\mu^-$  and  $4\mu$  modes. As can be seen in Fig. 5, the NWA works well inclusively for  $C_{ll}[1221]$  in both channels, though at the level of the differential distribution the agreement is worse, particularly beyond  $m_{Z^*} \gtrsim 34$  GeV.

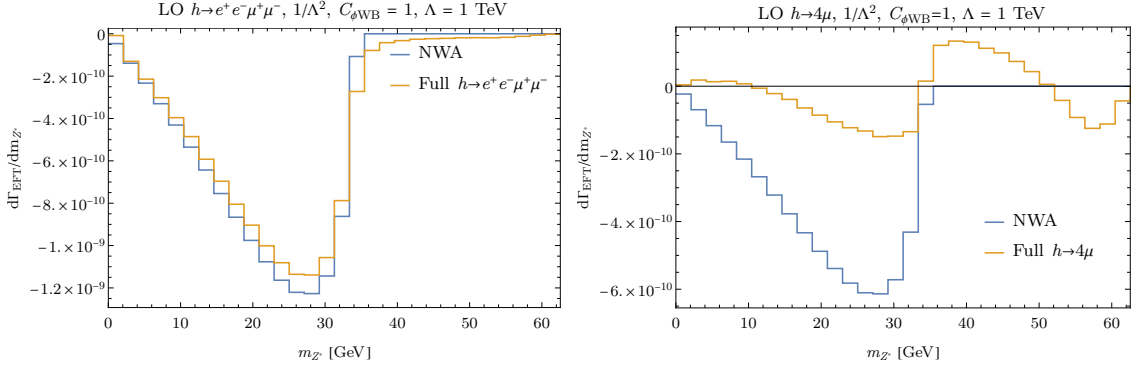


**Figure 6.** A comparison of the narrow width approximation and full  $h \rightarrow 4\ell$  results for  $C_{\phi WB}$ , where the narrow width approximation works for  $e^+e^-\mu^+\mu^-$  (left) but fails badly for the  $4\mu$  (right) channel. Here  $m_{Z^*}$  is defined to be the invariant mass of the opposite pair of same flavour opposite sign leptons from the pair with invariant mass closest to  $m_Z$ .

For many operators in the  $e^+e^-\mu^+\mu^-$  mode the agreement is actually quite good even differentially, as seen in Fig. 6. On the other hand, for the  $4\mu$  mode, neglected cross terms make the agreement worse, and it fails altogether for  $C_{\phi WB}$  where virtual photon contributions become important. No other coefficients fail as dramatically as  $C_{\phi WB}$ , but the large differences should be kept in mind when using these results.

An important consequence of having access to  $m_{\ell\ell}$  distributions is the ability to include the effect of the experimental cut  $m_{Z^*} \geq 12$  GeV used in the ATLAS and CMS analyses [26, 104, 105]. We include results with this cut in our numerical files at [31].

## 4 Results

In this section, we show some examples of the effects of NLO contributions to Higgs decays. In general, the NLO contributions offer a window into the effects of operators that do not appear at tree level, extending the physics reach of the HL-LHC program and future  $e^+e^-$  colliders. One of the major goals of these colliders is to measure the Higgs tri-linear coupling, as parameterized by  $C_\phi$  in the SMEFT, which first contributes to single Higgs production at one-loop order. It is hence important to understand the impact of a consistent calculation where all contributions are included at the same perturbative order.

### 4.1 HL-LHC projections

The inclusion of NLO SMEFT contributions provides sensitivity to operators that do not contribute to Higgs processes at LO. Attention has focussed largely on  $C_\phi$ , which generates anomalous Higgs tri-linear couplings [106–110]. When the full suite of dimension-6 SMEFT operators are included at NLO, the results become highly correlated [111]. The complete set of calculations required to compute Higgs production and decay to NLO electroweak/QCD order in the dimension-6 SMEFT at the LHC does not yet exist and so we include Higgs

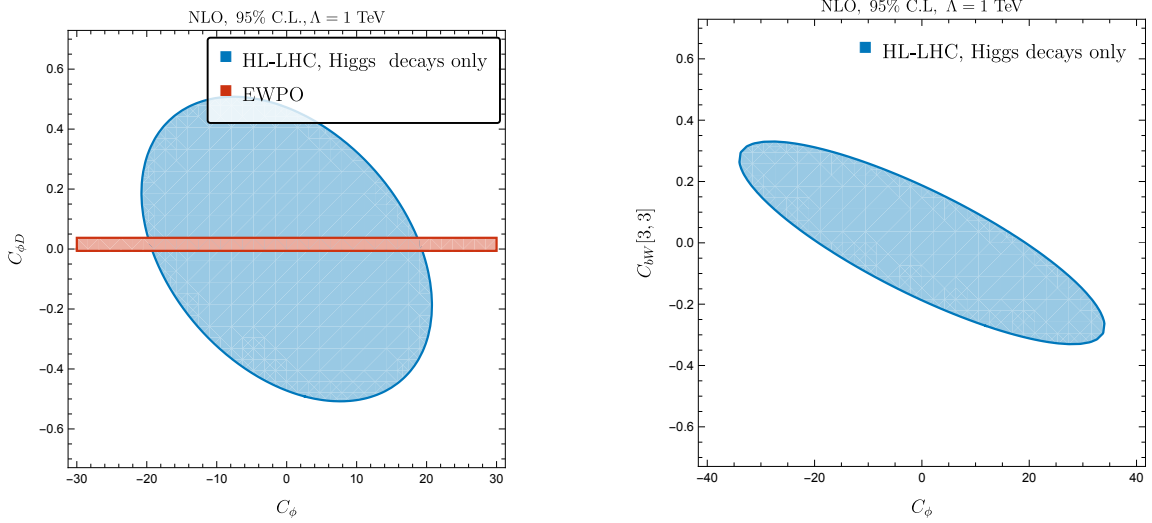


**Figure 7.** 95% C.L. limits from a complete NLO electroweak calculation of EWPOs [10], compared with HL-LHC projected limits, including the Higgs decay at NLO electroweak. Note that the operators in the right-hand plot are not constrained by EWPOs.

production channels calculated in the SM, followed by the full NLO Higgs decay predictions in the dimension-6 SMEFT. The results are hence only an indication of the impact of NLO electroweak corrections and motivate the complete calculation of production processes at NLO electroweak order for the LHC.

We assume that production and decay factorize at the HL-LHC ( $\mathcal{L} = 3 \text{ ab}^{-1}$ )<sup>12</sup> and further set the production processes to be given by the SM predictions. The Higgs decays are included at NLO in the dimension-6 SMEFT as described in this paper and are parameterized as

$$\mu_f = \frac{BR(h \rightarrow X_f)_{\text{SMEFT}}}{BR(h \rightarrow X_f)_{\text{SM}}} , \quad (4.1)$$

where  $X_f$  is the final state from the Higgs decay. We use the sensitivity projections of Ref. [112], along with the updates of Ref. [113]. We show in Fig. 7 the regions where  $\mu_f$ , summed over all production and decay modes is within 95% C.L. of the SM. On the left-hand side of Fig. 7, we show the correlation of  $C_\phi$  with  $C_{\phi D}$  and on the right-hand side, the correlation of  $C_\phi$  with  $C_{eu}$ [113]. The NLO accurate results from EWPOs (using the data of Tab. 1) are also shown, and we see that the combination of HL-LHC with EWPOs is highly restrictive. The right-hand side of Fig. 7 shows an example of two operators that do not contribute to EWPOs and demonstrates the strong correlation at HL-LHC. We note, however, that the NLO EW/QCD SMEFT contributions to the production processes need to be included in future studies in order to have NLO consistent results.

<sup>12</sup>This is not true for all dimension-6 operators.

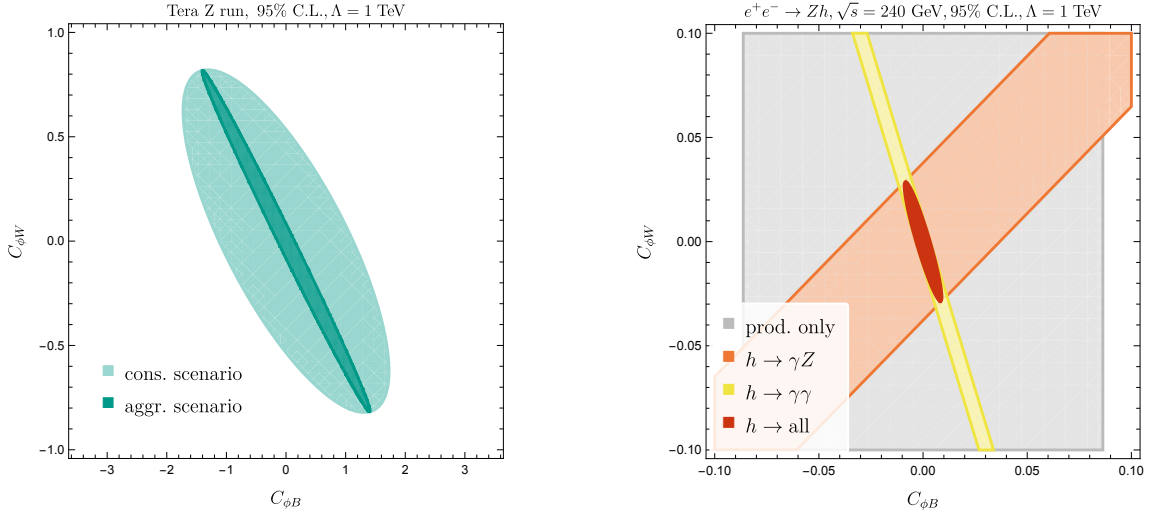


**Figure 8.** 95% confidence level (C.L.) sensitivities to  $C_{\phi B}$  and  $C_{\phi W}$ , for the Tera-Z run assuming either a conservative or aggressive set of theory uncertainties(left) and  $Zh$  production followed by the Higgs decays at  $\sqrt{s} = 240$  GeV (right).

#### 4.2 Comparing Tera-Z reach with Higgstrahlung Sensitivity

The NLO SMEFT results for Higgstrahlung production,  $e^+e^- \rightarrow Zh$ , can be combined with the NLO results for Higgs decays presented in this paper, and the NLO results for  $Z$  decays from Refs. [10, 12], to assess the expected sensitivities at future lepton colliders. We assume a relative precision of 0.5% for the total Higgstrahlung cross section at  $\sqrt{s} = 240$  GeV and use the projected sensitivities for Higgs decays at FCC-ee from Tab. 2 to derive 95% C.L. limits on pairs of dimension-6 SMEFT coefficients. These limits can be compared with those projected for the Tera-Z run, obtained from the electroweak precision observables listed in Tab. 3. To quantify the theoretical uncertainties we use the two scenarios defined in Ref. [114]: a conservative one, in which the errors are projected according to what is likely to be achieved by extending the present computational tools, and an aggressive one, in which it is assumed that fundamental advances in theory techniques and tools will considerably reduce the related uncertainties for most of the observables. We report the detailed numbers in Tab. 3.

We begin by considering in Fig. 8 pairs of operators that contribute to Higgstrahlung at tree-level, but enter  $Z$  production at the peak only at one-loop,  $C_{\phi B}$  and  $C_{\phi W}$ . The left-hand- side of the figure shows the limits derived at the Tera-Z run by adopting a conservative rather than an aggressive estimate of the theoretical uncertainties. We note the sensitivity of the result to the assumptions made about future theoretical uncertainties. The combined information from Higgs production and decays shown on the right-hand side allows an improvement of at least one order of magnitude on these sensitivities, two in the case of  $C_{\phi B}$ . In particular, the right-hand plot shows the complementary constraints given from the decay channels  $h \rightarrow \gamma Z$  and  $h \rightarrow \gamma\gamma$ , where the  $O_{\phi B}$  operator enters at leading order, while the coefficient of  $O_{\phi W}$ , which first appears at loop level, takes a different sign

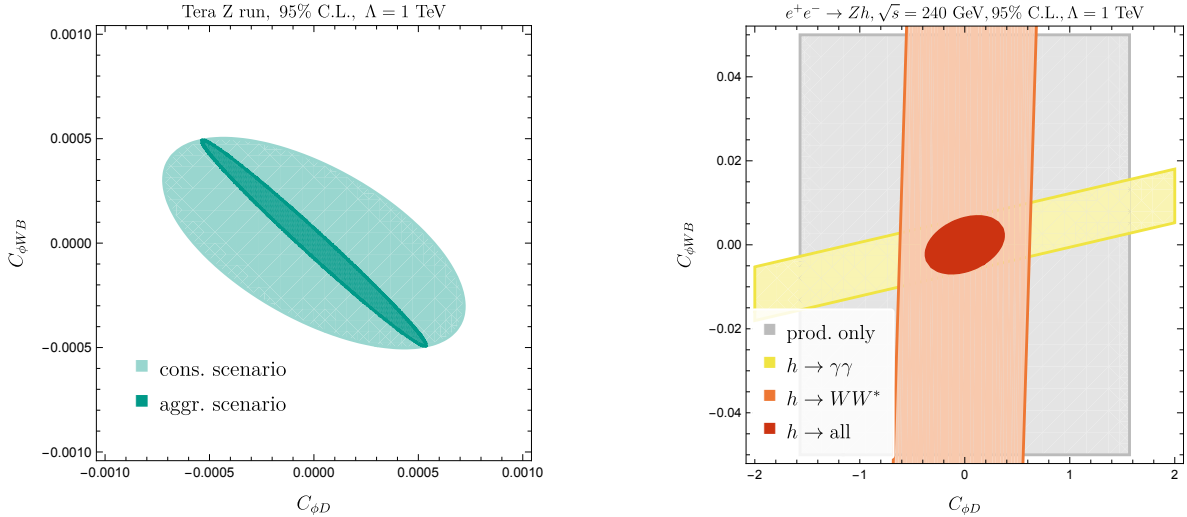


**Figure 9.** Same as Fig. 8, but with 95% C.L. limits on  $C_{\phi D}$  and  $C_{\phi WB}$ .

in the  $\gamma\gamma$  case, as compared to the  $\gamma Z$  one.

Fig. 9 illustrates the sensitivity to two operators entering at leading order in  $Z$  production,  $C_{\phi D}$  and  $C_{\phi WB}$ . In this case the higher statistics available at the Tera-Z run allows us to derive strong limits and it is apparent how tagging the Higgs decays enhances the constraining power of Higgstrahlung production alone. The  $h \rightarrow WW^*$  channel, computed here at NLO EW in the SMEFT for the first time, provides an order of magnitude improvement to the bound on  $C_{\phi D}$  as compared to that found from production only. However, the Higgstrahlung process is not competitive with the Tera-Z results for these operators. In Fig. 10 we present the sensitivity to  $C_\phi$  and  $C_{\phi\square}$  on the left and to the parameters  $\delta_Z$  and  $\delta\kappa_\lambda$  on the right. The linear dimension-6 SMEFT calculation has been reinterpreted in terms of  $\delta_Z$  and  $\delta\kappa_\lambda$ , parameterizing the deviations due to possible new physics in the  $hVV$  couplings and the Higgs self-interaction [102, 109, 110, 115, 116], via the relations [15]

$$\begin{aligned}\delta_Z &= \frac{1}{4} \frac{v^2}{\Lambda^2} \left( C_{\phi D} + 4C_{\phi\square} \right) \\ \delta\kappa_\lambda &= \frac{v^2}{\Lambda^2} \left( 3 \left[ \frac{C_{\phi D}}{4} - C_{\phi\square} \right] - 2 \frac{v^2}{m_h^2} C_\phi \right),\end{aligned}\quad (4.2)$$

where we set  $C_{\phi D} = 0$ . On the left-hand side, the 95% C.L. limits are derived by considering the Tera-Z run in green, and Higgsstrahlung production at  $\sqrt{s} = 240$  GeV in grey. Combining the latter with the information from Higgs decays is crucial for constraining  $C_\phi$ . On the right-hand side, we show the bounds obtained from production only by a joint fit of the runs at  $\sqrt{s} = 240$  and 365 GeV, where we assume a relative precision of 1% for the total Higgstrahlung cross section at  $\sqrt{s} = 365$  GeV. Lighter colors correspond to 95% C.L. and darker ones to 68% C.L. The red circles show how, when adding Higgs decay tagging on top of production, it is sufficient to run at a single energy to obtain much more robust

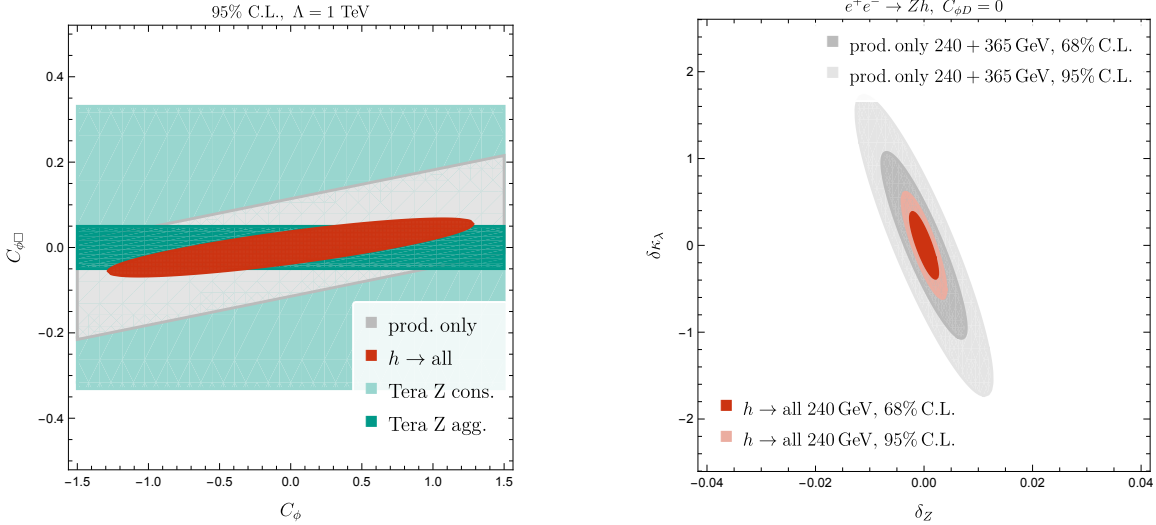


**Figure 10.** Bounds on coefficients contributing to  $hZZ/hWW$  and trilinear Higgs couplings. Left: SMEFT calculation in terms of  $C_\phi$  and  $C_{\phi\square}$ , with 95% C.L. sensitivities from Higgsstrahlung with (without) the Higgs decays in red (grey) and from the Tera-Z run in green with aggressive and conservative assumptions about theory uncertainties. Right: Interpretation in terms of the  $\delta_Z$  and  $\delta\kappa_\lambda$  parameters computed at linear order, considering  $C_{\phi D} = 0$ . Limits at 68% and 95% C.L. are given by combining by combining two energy runs at  $\sqrt{s} = 240$  and 365 GeV (grey) with only the total cross section included and by considering Higgstrahlung with Higgs decays included at a single energy,  $\sqrt{s} = 240$  GeV (red/pink).

limits than from total cross section measurements alone. This plot can be compared to Fig. 4 of Ref. [17], which is obtained by setting  $C_{\phi\square} = 0$  and plotting  $C_{\phi D}$  vs.  $C_\phi$ . Given that  $C_{\phi\square}$  is very well constrained, the derived limits on  $\delta_Z$  and  $\delta\kappa_\lambda$  are more stringent in the  $C_{\phi\square} - C_\phi$  fit.

For operators that contribute to  $e^+e^-b\bar{b}$  and  $e^+e^-t\bar{t}$  interactions at tree level, the measurements of  $e^+e^- \rightarrow b\bar{b}$  above the  $Z$  pole and of  $e^+e^- \rightarrow t\bar{t}$  at the  $t\bar{t}$  threshold can significantly reduce the allowed parameter space for these coefficients [117–120]. Interestingly, a measurement of  $R_t$  at the  $t\bar{t}$  threshold effectively eliminates the correlation between  $C_\phi$  and the five  $e^+e^-b\bar{b}$  and  $e^+e^-t\bar{t}$  operators [120].

### 4.3 Case Study: Scalar Singlet Model

It is interesting to examine the effects of NLO corrections to the Higgstrahlung process and compare them with those resulting from Tera-Z data. As a test case, we study the BSM model with a single heavy neutral scalar particle,  $S$ , added to the SM [121–123]. This model serves to illustrate many of the assumptions that go into deriving conclusions about the discovery reach of future colliders. The scalar singlet model is highly motivated since it can generate a first order electroweak phase transition for some choices of the parameters [124, 125].

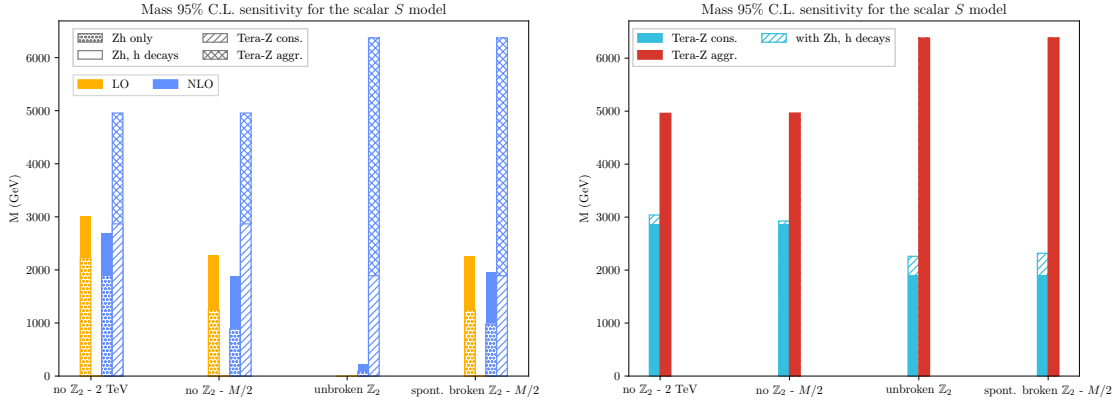


**Figure 11.** 95% C.L. mass reach for the  $S$  model under the different symmetry hypotheses discussed in the text. The labels 2 TeV and  $M/2$  refer to the assumptions on dimensional parameters discussed in the main text. Left:  $e^+e^- \rightarrow Zh$  at  $\sqrt{s} = 240$  GeV (dots), Higgsstrahlung combined with Higgs decays (solid), the Tera-Z data in the conservative (stripes) and aggressive scenarios (crosses). The matching is performed at LO (yellow) and NLO (blue). Right: NLO matching considering the Tera-Z conservative (light blue) and aggressive (red) uncertainty scenarios combined with the run at  $\sqrt{s} = 240$  GeV including Higgsstrahlung and the Higgs decays (stripes).

The most general potential coupling a gauge singlet scalar,  $S$ , to the SM Higgs doublet,  $\Phi^T = (\phi^+, \phi^0)$  is,

$$V(\Phi, S) = -\mu_H^2 \Phi^\dagger \Phi + \lambda_H (\Phi^\dagger \Phi)^2 + \frac{m_\xi^2}{2} \Phi^\dagger \Phi S + \frac{\kappa}{2} \Phi^\dagger \Phi S^2 + t_S S + \frac{M^2}{2} S^2 + \frac{m_\zeta^2}{3} S^3 + \frac{\lambda_S}{4} S^4. \quad (4.3)$$

There are two distinct cases: The model possesses a  $\mathbb{Z}_2$  symmetry, in which case  $m_\zeta = t_S = m_\xi = 0$  or there is no  $\mathbb{Z}_2$  symmetry in which case  $S$  can obtain a non-zero vev and the Lagrangian parameters can be shifted to eliminate the tadpole term,  $t_S$ . The physical scalars,  $h_1$  and  $h_2$ , are admixtures of  $S$  and  $\phi^0$ , and we will assume that  $h_1 = h$  is the SM Higgs boson, while  $h_2$  is much heavier.

It is straightforward to match the singlet model to the dimension-6 SMEFT at tree-level by taking the limit  $m_{h_2} \rightarrow \infty$ . In this limit,  $m_{h_2} \rightarrow M$  and two SMEFT coefficients are generated at tree level,

$$O_\phi = |\Phi^\dagger \Phi|^3 \quad (4.4)$$

$$O_{\phi\square} = |\Phi^\dagger \Phi| \square |\Phi^\dagger \Phi|. \quad (4.5)$$

There are 3 possibilities for the pattern of coefficients [122, 126, 127]:

- The  $\mathbb{Z}_2$  symmetry remains unbroken in which case no operators are generated at tree-

level. At one-loop level,  $O_\phi$  and  $O_{\phi\square}$  are generated with coefficients:

$$\begin{aligned} C_\phi &= -\frac{\kappa^3}{192\pi^2} \\ C_{\phi\square} &= -\frac{\kappa^2}{384\pi^2}. \end{aligned} \quad (4.6)$$

- The  $\mathbb{Z}_2$  symmetry can be spontaneously broken and the  $\mathbb{Z}_2$  symmetry implies the relationship,  $\kappa = \frac{m_\zeta m_\xi}{3M^2}$ . At tree- level:

$$\begin{aligned} C_\phi &= 0 \\ C_{\phi\square} &= -\frac{m_\xi^2}{8M^2}. \end{aligned} \quad (4.7)$$

- If there is no  $\mathbb{Z}_2$  symmetry, the tree level contributions are,

$$\begin{aligned} C_\phi &= \frac{m_\xi^2}{8M^2} \left[ \frac{m_\zeta m_\xi}{3M^2} - \kappa \right] \\ C_{\phi\square} &= -\frac{m_\xi^2}{8M^2}. \end{aligned} \quad (4.8)$$

In the numerical results for the matching, we set all dimensionless parameters in the UV-complete model to one, while discussing possible choices for the dimensional quantities.

Fig. 11 shows the 95% C.L. mass reach for the  $S$  model under these different symmetry assumptions. In the left panel, dotted columns refer to fitting only the total cross section for  $e^+e^- \rightarrow Zh$  at  $\sqrt{s} = 240$  GeV, while solid colors correspond to Higgstrahlung production combined with Higgs decays. Single- and double-striped hatches denote the Tera-Z run in the conservative and aggressive uncertainty scenarios, respectively. The colors identify the order of the matching: LO in yellow and NLO in blue. For consistency, the accuracy of the observables used in this analysis is always the same as the matching procedure.

Let us first consider the case with the no  $\mathbb{Z}_2$  symmetry hypothesis. To translate the matching equations into mass limits, we always set dimensionless parameters of the UV model to one, and then need to make some assumption on the dimensional coefficients of the complete theory. In the literature, common choices are  $m_\xi/2 = m_\zeta/3 = 1$  TeV or  $m_\xi/2 = m_\zeta/3 = 2$  TeV, and we present the latter in the plot. The resulting mass reach is however not always higher than 2 TeV, invalidating the expansion in  $m/M$ , with  $m$  a generic dimensional coefficient of the complete model, that is assumed in the matching. We therefore adopt the assumption  $m_\xi/2 = m_\zeta/3 = M/2$  and fit  $M$ . The limits derived within this hypothesis are considerably different from the ones obtained by setting  $m_\xi/2 = m_\zeta/3 = 2$  TeV, if the matching is not performed considering the NLO complete calculation. This demonstrates the impact of assumptions about the dimensional couplings on the projected mass reach limits.

The case of spontaneously broken  $\mathbb{Z}_2$  symmetry is similar, because the fit is driven by  $C_{\phi\square}$ , which is much more constrained than  $C_\phi$ , as can be seen in the left-hand panel of Fig. 10.

In addition, Tera-Z data has no sensitivity to  $C_\phi$ . In general, one can observe that the information from Higgs production combined with the decays and from the Tera-Z data provide similar bounds, since the higher statistics available at the  $Z$  peak compensates the lack of sensitivity on  $C_\phi$ .

Finally, we assume that the  $\mathbb{Z}_2$  symmetry is left unbroken, and  $O_\phi$  and  $O_{\phi\square}$  are generated first at one-loop. In this case, the higher statistics from the  $Z$  peak gives the strongest limits on the  $S$  model.

The right-hand panel of Fig. 11 shows the mass reach once the data from the Tera-Z run have been combined with the data coming from Higgsstrahlung plus decays. As expected from their relative size, the combination of the bounds from Higgs processes with those of the conservative scenario yields a slight improvement with respect to that of the Tera-Z run alone. On the other hand, no appreciable improvement from the Higgstrahlung data can be seen in the aggressive theory scenario.

## 5 Conclusions

We have computed all two- and three-body Higgs decays at NLO in the dimension-6 SMEFT. The physical four-body final states  $h \rightarrow (f_1 \bar{f}_2)(f_3 \bar{f}_4)$  are determined by using the exact four-body SMEFT result for the LO contribution and including the NLO contribution by combining the NLO  $h \rightarrow V(f_1 \bar{f}_2)$  result with the NLO result for  $V \rightarrow (f_3 \bar{f}_4)$  using the NWA. The results are contained in the publicly available Monte Carlo code NEWiSH [31] and numerical results are provided both in the text and at the [GitLab repository](#), allowing for the NLO EW/QCD evaluation of Higgs branching ratios to  $\mathcal{O}\left(\frac{1}{(4\pi\Lambda)^2}\right)$  in the dimension-6 SMEFT.

The effects of NLO corrections are largely to induce correlations between operator contributions to observables, implying that great care is required in interpreting single parameter limits. We demonstrate that by combining results from Tera-Z with data from Higgstrahlung, many of these ambiguities can be resolved. For operators that contribute to Tera-Z at tree level, including the Higgstrahlung data with Higgs decays to NLO EW order gives only a small improvement to the sensitivity from Tera-Z results alone in the cases we have studied. However, for operators that do not contribute to Tera-Z at tree level, the Higgstrahlung measurements combined with the NLO Higgs decays can result in significantly improved sensitivity. We can therefore anticipate interesting effects when incorporating the results presented here into global analyses.

Most of our conclusions depend sensitively on the assumptions about SM theory uncertainties, demonstrating the need for more precise theoretical calculations. In a similar fashion as in Ref. [114], we considered two scenarios for the theoretical uncertainties of the future Tera-Z run, corresponding to different levels of theoretical progress and technological advancement. As a test case, we examined the Tera-Z reach for a scalar singlet and observed that the mass bound differs depending on the assumptions about the  $Z_2$  symmetry of the potential and the numerical values of the dimensional parameters. In this example, the

Higgstrahlung data slightly improve the projected mass reach obtained from the Tera-Z run only in the conservative scenario for theory uncertainties, while no meaningful improvement from Higgstrahlung measurements can be observed in the aggressive scenario.

These results highlight an important point. Under conservative assumptions, the Tera-Z run offers only limited improvement over other FCC-ee runs in probing BSM physics. By contrast, the aggressive scenario is expected to deliver markedly greater advances. This clearly demonstrates the need for the theoretical community to push towards the development of new technologies and methods in order to reach the level of precision required to fully take advantage of the FCC-ee.

The extraction of SMEFT coefficients from HL-LHC data is a crucial tool in the search for high scale new physics. Our work represents an important step toward NLO electroweak/QCD accurate predictions in the dimension-6 SMEFT, but a complete calculation including Higgs production processes at the LHC is needed for accurate global fits. Furthermore, the complete NLO calculation of  $h \rightarrow 4f$  without using the NWA is also a necessary ingredient for increasing the precision of future SMEFT studies.

## Acknowledgments

We would like to thank Marvin Schnubel for naming inspiration of the NEWiSH code. S. D. and C.D.P. are supported by the U.S. Department of Energy under Contract No. DE-SC0012704. P.P.G. is supported by the Ramón y Cajal grant RYC2022-038517-I funded by MCIN/AEI/10.13039/501100011033 and by FSE+, and by the Spanish Research Agency (Agencia Estatal de Investigación) through the grant IFT Centro de Excelencia Severo Ochoa No CEX2020-001007-S. The work of L.B. is supported in part by the U.S. Department of Energy under Grant No. DE-SC0010102 and by the College of Arts and Sciences of Florida State University. L.B. thanks the Technische Universität München (TUM) for the hospitality and the Excellence Cluster ORIGINS which is funded by the Deutsche Forschungsgemeinschaft (DFG, German Research Foundation) under Germany’s Excellence Strategy – EXC-2094 – 390783311 for partial support during the completion of this work. Digital data including partial widths and the code NEWiSH is provided at a [GitLab](#)  repository.

## References

- [1] **CMS** Collaboration, A. Tumasyan *et al.*, “A portrait of the Higgs boson by the CMS experiment ten years after the discovery,” *Nature* **607** no. 7917, (2022) 60–68, [arXiv:2207.00043 \[hep-ex\]](https://arxiv.org/abs/2207.00043). [Erratum: *Nature* 623, (2023)].
- [2] **ATLAS** Collaboration, G. Aad *et al.*, “A detailed map of Higgs boson interactions by the ATLAS experiment ten years after the discovery,” *Nature* **607** no. 7917, (2022) 52–59, [arXiv:2207.00092 \[hep-ex\]](https://arxiv.org/abs/2207.00092). [Erratum: *Nature* 612, E24 (2022)].
- [3] **ATLAS** Collaboration, “Highlights of the HL-LHC physics projections by ATLAS and CMS,” tech. rep., CERN, Geneva, 2025. <https://cds.cern.ch/record/2928907>. All

figures including auxiliary figures are available at  
<https://atlas.web.cern.ch/Atlas/GROUPS/PHYSICS/PUBNOTES/ATL-PHYS-PUB-2025-018>.

- [4] A. Huss, J. Huston, S. Jones, M. Pellen, and R. Röntsch, “Les Houches 2023 – Physics at TeV Colliders: Report on the Standard Model Precision Wishlist,” [arXiv:2504.06689](https://arxiv.org/abs/2504.06689) [hep-ph].
- [5] A. Blondel, J. Gluza, S. Jadach, P. Janot, and T. Riemann, eds., *Theory for the FCC-ee: Report on the 11th FCC-ee Workshop Theory and Experiments*, vol. 3/2020 of *CERN Yellow Reports: Monographs*. CERN, Geneva, 5, 2019. [arXiv:1905.05078](https://arxiv.org/abs/1905.05078) [hep-ph].
- [6] M. Spira, “Higgs Boson Production and Decay at Hadron Colliders,” *Prog. Part. Nucl. Phys.* **95** (2017) 98–159, [arXiv:1612.07651](https://arxiv.org/abs/1612.07651) [hep-ph].
- [7] I. Brivio and M. Trott, “The Standard Model as an Effective Field Theory,” *Phys. Rept.* **793** (2019) 1–98, [arXiv:1706.08945](https://arxiv.org/abs/1706.08945) [hep-ph].
- [8] I. Brivio, “SMEFTsim 3.0 — a practical guide,” *JHEP* **04** (2021) 073, [arXiv:2012.11343](https://arxiv.org/abs/2012.11343) [hep-ph].
- [9] C. Degrande, G. Durieux, F. Maltoni, K. Mimasu, E. Vryonidou, and C. Zhang, “Automated one-loop computations in the standard model effective field theory,” *Phys. Rev. D* **103** no. 9, (2021) 096024, [arXiv:2008.11743](https://arxiv.org/abs/2008.11743) [hep-ph].
- [10] L. Bellafronte, S. Dawson, and P. P. Giardino, “The importance of flavor in SMEFT Electroweak Precision Fits,” *JHEP* **05** (2023) 208, [arXiv:2304.00029](https://arxiv.org/abs/2304.00029) [hep-ph].
- [11] S. Dawson and P. P. Giardino, “Electroweak and QCD corrections to  $Z$  and  $W$  pole observables in the standard model EFT,” *Phys. Rev. D* **101** no. 1, (2020) 013001, [arXiv:1909.02000](https://arxiv.org/abs/1909.02000) [hep-ph].
- [12] A. Biekötter and B. D. Pecjak, “Analytic results for electroweak precision observables at NLO in SMEFT,” *JHEP* **07** (2025) 134, [arXiv:2503.07724](https://arxiv.org/abs/2503.07724) [hep-ph].
- [13] S. Dawson, P. P. Giardino, and A. Ismail, “Standard model EFT and the Drell-Yan process at high energy,” *Phys. Rev. D* **99** no. 3, (2019) 035044, [arXiv:1811.12260](https://arxiv.org/abs/1811.12260) [hep-ph].
- [14] S. Dawson and P. P. Giardino, “New physics through Drell-Yan standard model EFT measurements at NLO,” *Phys. Rev. D* **104** no. 7, (2021) 073004, [arXiv:2105.05852](https://arxiv.org/abs/2105.05852) [hep-ph].
- [15] K. Asteriadis, S. Dawson, P. P. Giardino, and R. Szafron, “ $e^+e^- \rightarrow ZH$  process in the SMEFT beyond leading order,” *JHEP* **02** (2025) 162, [arXiv:2409.11466](https://arxiv.org/abs/2409.11466) [hep-ph].
- [16] K. Asteriadis, S. Dawson, P. P. Giardino, and R. Szafron, “Impact of Next-to-Leading-Order Weak Standard-Model-Effective-Field-Theory Corrections in  $e^+e^- \rightarrow ZH$ ,” *Phys. Rev. Lett.* **133** no. 23, (2024) 231801, [arXiv:2406.03557](https://arxiv.org/abs/2406.03557) [hep-ph].
- [17] L. Bellafronte, S. Dawson, C. Del Pio, M. Forslund, and P. P. Giardino, “Complete NLO SMEFT Electroweak Corrections to Higgs Decays,” [arXiv:2508.14966](https://arxiv.org/abs/2508.14966) [hep-ph].
- [18] J. M. Cullen and B. D. Pecjak, “Higgs decay to fermion pairs at NLO in SMEFT,” *JHEP* **11** (2020) 079, [arXiv:2007.15238](https://arxiv.org/abs/2007.15238) [hep-ph].
- [19] J. M. Cullen, B. D. Pecjak, and D. J. Scott, “NLO corrections to  $h \rightarrow b\bar{b}$  decay in SMEFT,” *JHEP* **08** (2019) 173, [arXiv:1904.06358](https://arxiv.org/abs/1904.06358) [hep-ph].

[20] R. Gauld, B. D. Pecjak, and D. J. Scott, “QCD radiative corrections for  $h \rightarrow b\bar{b}$  in the Standard Model Dimension-6 EFT,” *Phys. Rev. D* **94** no. 7, (2016) 074045, [arXiv:1607.06354 \[hep-ph\]](https://arxiv.org/abs/1607.06354).

[21] S. Dawson and P. P. Giardino, “Higgs decays to  $ZZ$  and  $Z\gamma$  in the standard model effective field theory: An NLO analysis,” *Phys. Rev. D* **97** no. 9, (2018) 093003, [arXiv:1801.01136 \[hep-ph\]](https://arxiv.org/abs/1801.01136).

[22] A. Dedes, K. Suxho, and L. Trifyllis, “The decay  $h \rightarrow Z\gamma$  in the Standard-Model Effective Field Theory,” *JHEP* **06** (2019) 115, [arXiv:1903.12046 \[hep-ph\]](https://arxiv.org/abs/1903.12046).

[23] S. Dawson and P. P. Giardino, “Electroweak corrections to Higgs boson decays to  $\gamma\gamma$  and  $W^+W^-$  in standard model EFT,” *Phys. Rev. D* **98** no. 9, (2018) 095005, [arXiv:1807.11504 \[hep-ph\]](https://arxiv.org/abs/1807.11504).

[24] A. Dedes, M. Paraskevas, J. Rosiek, K. Suxho, and L. Trifyllis, “The decay  $h \rightarrow \gamma\gamma$  in the Standard-Model Effective Field Theory,” *JHEP* **08** (2018) 103, [arXiv:1805.00302 \[hep-ph\]](https://arxiv.org/abs/1805.00302).

[25] C. Hartmann and M. Trott, “Higgs Decay to Two Photons at One Loop in the Standard Model Effective Field Theory,” *Phys. Rev. Lett.* **115** no. 19, (2015) 191801, [arXiv:1507.03568 \[hep-ph\]](https://arxiv.org/abs/1507.03568).

[26] S. Dawson, M. Forslund, and P. P. Giardino, “NLO SMEFT electroweak corrections to Higgs boson decays to four leptons in the narrow width approximation,” *Phys. Rev. D* **111** no. 1, (2025) 015016, [arXiv:2411.08952 \[hep-ph\]](https://arxiv.org/abs/2411.08952).

[27] A. Martin and M. Trott, “More accurate  $\sigma(\mathcal{G}\mathcal{G} \rightarrow h), \Gamma(h \rightarrow \mathcal{G}\mathcal{G}, \mathcal{A}\mathcal{A}, \bar{\Psi}\Psi)$  and Higgs width results via the geoSMEFT,” *JHEP* **01** (2024) 170, [arXiv:2305.05879 \[hep-ph\]](https://arxiv.org/abs/2305.05879).

[28] T. Corbett, A. Martin, and M. Trott, “Consistent higher order  $\sigma(\mathcal{G}\mathcal{G} \rightarrow h), \Gamma(h \rightarrow \mathcal{G}\mathcal{G})$  and  $\Gamma(h \rightarrow \gamma\gamma)$  in geoSMEFT,” *JHEP* **12** (2021) 147, [arXiv:2107.07470 \[hep-ph\]](https://arxiv.org/abs/2107.07470).

[29] L. Born, J. Fuentes-Martín, S. Kvedaraitė, and A. E. Thomsen, “Two-loop running in the bosonic SMEFT using functional methods,” *JHEP* **05** (2025) 121, [arXiv:2410.07320 \[hep-ph\]](https://arxiv.org/abs/2410.07320).

[30] A. Greljo, A. Palavrić, and A. E. Thomsen, “Adding Flavor to the SMEFT,” *JHEP* **10** (2022) 010, [arXiv:2203.09561 \[hep-ph\]](https://arxiv.org/abs/2203.09561).

[31] L. Bellafronte, S. Dawson, C. Del Pio, M. Forslund, and P. P. Giardino, “NEWiSH: NLO ElectroWeak in the SMEFT for Higgs widths,” <https://gitlab.com/mforslund/newish>, 2025.

[32] B. Grzadkowski, M. Iskrzynski, M. Misiak, and J. Rosiek, “Dimension-Six Terms in the Standard Model Lagrangian,” *JHEP* **10** (2010) 085, [arXiv:1008.4884 \[hep-ph\]](https://arxiv.org/abs/1008.4884).

[33] A. Dedes, W. MATERKOWSKA, M. Paraskevas, J. Rosiek, and K. Suxho, “Feynman rules for the Standard Model Effective Field Theory in  $R_\xi$ -gauges,” *JHEP* **06** (2017) 143, [arXiv:1704.03888 \[hep-ph\]](https://arxiv.org/abs/1704.03888).

[34] A. Alloul, N. D. Christensen, C. Degrande, C. Duhr, and B. Fuks, “FeynRules 2.0 - A complete toolbox for tree-level phenomenology,” *Comput. Phys. Commun.* **185** (2014) 2250–2300, [arXiv:1310.1921 \[hep-ph\]](https://arxiv.org/abs/1310.1921).

[35] T. Hahn, “Generating Feynman diagrams and amplitudes with FeynArts 3,” *Comput. Phys. Commun.* **140** (2001) 418–431, [arXiv:hep-ph/0012260](https://arxiv.org/abs/hep-ph/0012260).

[36] V. Shtabovenko, R. Mertig, and F. Orellana, “FeynCalc 10: Do multiloop integrals dream of computer codes?,” *Comput. Phys. Commun.* **306** (2025) 109357, [arXiv:2312.14089 \[hep-ph\]](https://arxiv.org/abs/2312.14089).

[37] G. Passarino and M. J. G. Veltman, “One Loop Corrections for  $e^+e^-$  Annihilation Into  $\mu^+\mu^-$  in the Weinberg Model,” *Nucl. Phys. B* **160** (1979) 151–207.

[38] H. H. Patel, “Package-X 2.0: A Mathematica package for the analytic calculation of one-loop integrals,” *Comput. Phys. Commun.* **218** (2017) 66–70, [arXiv:1612.00009 \[hep-ph\]](https://arxiv.org/abs/1612.00009).

[39] A. Denner, S. Dittmaier, and L. Hofer, “Collier: a fortran-based Complex One-Loop Library in Extended Regularizations,” *Comput. Phys. Commun.* **212** (2017) 220–238, [arXiv:1604.06792 \[hep-ph\]](https://arxiv.org/abs/1604.06792).

[40] A. Denner and S. Dittmaier, “The Complex-mass scheme for perturbative calculations with unstable particles,” *Nucl. Phys. B Proc. Suppl.* **160** (2006) 22–26, [arXiv:hep-ph/0605312](https://arxiv.org/abs/hep-ph/0605312).

[41] S. Dittmaier and M. Huber, “Radiative corrections to the neutral-current Drell-Yan process in the Standard Model and its minimal supersymmetric extension,” *JHEP* **01** (2010) 060, [arXiv:0911.2329 \[hep-ph\]](https://arxiv.org/abs/0911.2329).

[42] I. Brivio, T. Corbett, and M. Trott, “The Higgs width in the SMEFT,” *JHEP* **10** (2019) 056, [arXiv:1906.06949 \[hep-ph\]](https://arxiv.org/abs/1906.06949).

[43] A. Denner and S. Dittmaier, “Electroweak Radiative Corrections for Collider Physics,” *Phys. Rept.* **864** (2020) 1–163, [arXiv:1912.06823 \[hep-ph\]](https://arxiv.org/abs/1912.06823).

[44] A. Sirlin, “Radiative Corrections in the  $SU(2)_L \times U(1)$  Theory: A Simple Renormalization Framework,” *Phys. Rev. D* **22** (1980) 971–981.

[45] W. J. Marciano and A. Sirlin, “Radiative Corrections to Neutrino Induced Neutral Current Phenomena in the  $SU(2)_L \times U(1)$  Theory,” *Phys. Rev. D* **22** (1980) 2695. [Erratum: Phys. Rev. D 31, 213 (1985)].

[46] E. E. Jenkins, A. V. Manohar, and M. Trott, “Renormalization Group Evolution of the Standard Model Dimension Six Operators I: Formalism and lambda Dependence,” *JHEP* **10** (2013) 087, [arXiv:1308.2627 \[hep-ph\]](https://arxiv.org/abs/1308.2627).

[47] E. E. Jenkins, A. V. Manohar, and M. Trott, “Renormalization Group Evolution of the Standard Model Dimension Six Operators II: Yukawa Dependence,” *JHEP* **01** (2014) 035, [arXiv:1310.4838 \[hep-ph\]](https://arxiv.org/abs/1310.4838).

[48] R. Alonso, E. E. Jenkins, A. V. Manohar, and M. Trott, “Renormalization Group Evolution of the Standard Model Dimension Six Operators III: Gauge Coupling Dependence and Phenomenology,” *JHEP* **04** (2014) 159, [arXiv:1312.2014 \[hep-ph\]](https://arxiv.org/abs/1312.2014).

[49] R. Alonso, H.-M. Chang, E. E. Jenkins, A. V. Manohar, and B. Shotwell, “Renormalization group evolution of dimension-six baryon number violating operators,” *Phys. Lett. B* **734** (2014) 302–307, [arXiv:1405.0486 \[hep-ph\]](https://arxiv.org/abs/1405.0486).

[50] J. ter Hoeve, L. Mantani, J. Rojo, A. N. Rossia, and E. Vryonidou, “Connecting scales: RGE effects in the SMEFT at the LHC and future colliders,” *JHEP* **06** (2025) 125, [arXiv:2502.20453 \[hep-ph\]](https://arxiv.org/abs/2502.20453).

[51] R. Bartocci, A. Biekötter, and T. Hurth, “Renormalisation group evolution effects on global SMEFT analyses,” *JHEP* **05** (2025) 203, [arXiv:2412.09674 \[hep-ph\]](https://arxiv.org/abs/2412.09674).

[52] S. Catani and M. H. Seymour, “A General algorithm for calculating jet cross-sections in NLO QCD,” *Nucl. Phys. B* **485** (1997) 291–419, [arXiv:hep-ph/9605323](https://arxiv.org/abs/hep-ph/9605323). [Erratum: Nucl.Phys.B 510, 503–504 (1998)].

[53] S. Dittmaier, “A General approach to photon radiation off fermions,” *Nucl. Phys. B* **565** (2000) 69–122, [arXiv:hep-ph/9904440](https://arxiv.org/abs/hep-ph/9904440).

[54] S. Catani, S. Dittmaier, M. H. Seymour, and Z. Trocsanyi, “The Dipole formalism for next-to-leading order QCD calculations with massive partons,” *Nucl. Phys. B* **627** (2002) 189–265, [arXiv:hep-ph/0201036](https://arxiv.org/abs/hep-ph/0201036).

[55] A. Freitas, Q. Song, and K. Xie, “Fermionic electroweak NNLO corrections to  $e^+e^- \rightarrow ZH$  with polarized beams and different renormalization schemes,” *Phys. Rev. D* **108** no. 5, (2023) 053006, [arXiv:2305.16547 \[hep-ph\]](https://arxiv.org/abs/2305.16547).

[56] D. Y. Bardin, A. Leike, T. Riemann, and M. Sachwitz, “Energy Dependent Width Effects in  $e^+e^-$  Annihilation Near the Z Boson Pole,” *Phys. Lett. B* **206** (1988) 539–542.

[57] **LHC Higgs Cross Section Working Group** Collaboration, D. de Florian *et al.*, “Handbook of LHC Higgs Cross Sections: 4. Deciphering the Nature of the Higgs Sector,” *CERN Yellow Rep. Monogr.* **2** (2017) 1–869, [arXiv:1610.07922 \[hep-ph\]](https://arxiv.org/abs/1610.07922).

[58] **Particle Data Group** Collaboration, S. Navas *et al.*, “Review of particle physics,” *Phys. Rev. D* **110** no. 3, (2024) 030001.

[59] D. d’Enterria and V. D. Le, “Rare few-body decays of the Standard Model Higgs boson,” [arXiv:2508.00466 \[hep-ph\]](https://arxiv.org/abs/2508.00466).

[60] N. Deutschmann, C. Duhr, F. Maltoni, and E. Vryonidou, “Gluon-fusion Higgs production in the Standard Model Effective Field Theory,” *JHEP* **12** (2017) 063, [arXiv:1708.00460 \[hep-ph\]](https://arxiv.org/abs/1708.00460). [Erratum: JHEP 02, 159 (2018)].

[61] K. Asteriadis, S. Dawson, and D. Fontes, “Double insertions of SMEFT operators in gluon fusion Higgs boson production,” *Phys. Rev. D* **107** no. 5, (2023) 055038, [arXiv:2212.03258 \[hep-ph\]](https://arxiv.org/abs/2212.03258).

[62] S. Boselli, C. M. Carloni Calame, G. Montagna, O. Nicrosini, and F. Piccinini, “Higgs boson decay into four leptons at NLOPS electroweak accuracy,” *JHEP* **06** (2015) 023, [arXiv:1503.07394 \[hep-ph\]](https://arxiv.org/abs/1503.07394).

[63] M. Kaur, M. Mahakhud, A. Shivaji, and X. Zhao, “QCD corrections to the Golden decay channel of the Higgs boson,” *JHEP* **04** (2024) 069, [arXiv:2307.16063 \[hep-ph\]](https://arxiv.org/abs/2307.16063).

[64] A. Bredenstein, A. Denner, S. Dittmaier, and M. M. Weber, “Precise predictions for the Higgs-boson decay  $H \rightarrow WW/ZZ \rightarrow 4$  leptons,” *Phys. Rev. D* **74** (2006) 013004, [arXiv:hep-ph/0604011](https://arxiv.org/abs/hep-ph/0604011).

[65] A. Bredenstein, A. Denner, S. Dittmaier, and M. M. Weber, “Radiative corrections to the semileptonic and hadronic Higgs-boson decays  $H \rightarrow WW/ZZ \rightarrow 4f$ ,” *JHEP* **02** (2007) 080, [arXiv:hep-ph/0611234](https://arxiv.org/abs/hep-ph/0611234).

[66] A. Denner, S. Dittmaier, and A. Mück, “PROPHECY4F 3.0: A Monte Carlo program for Higgs-boson decays into four-fermion final states in and beyond the Standard Model,” *Comput. Phys. Commun.* **254** (2020) 107336, [arXiv:1912.02010 \[hep-ph\]](https://arxiv.org/abs/1912.02010).

[67] **HDECAY** Collaboration, A. Djouadi, J. Kalinowski, M. Muehlleitner, and M. Spira, “HDECAY: Twenty<sub>++</sub> years after,” *Comput. Phys. Commun.* **238** (2019) 214–231, [arXiv:1801.09506 \[hep-ph\]](https://arxiv.org/abs/1801.09506).

[68] J. H. Kuhn, A. Kulesza, S. Pozzorini, and M. Schulze, “Electroweak corrections to hadronic production of W bosons at large transverse momenta,” *Nucl. Phys. B* **797** (2008) 27–77, [arXiv:0708.0476 \[hep-ph\]](https://arxiv.org/abs/0708.0476).

[69] W. Bernreuther, L. Chen, and Z.-G. Si, “Differential decay rates of CP-even and CP-odd Higgs bosons to top and bottom quarks at NNLO QCD,” *JHEP* **07** (2018) 159, [arXiv:1805.06658 \[hep-ph\]](https://arxiv.org/abs/1805.06658).

[70] A. Primo, G. Sasso, G. Somogyi, and F. Tramontano, “Exact Top Yukawa corrections to Higgs boson decay into bottom quarks,” *Phys. Rev. D* **99** no. 5, (2019) 054013, [arXiv:1812.07811 \[hep-ph\]](https://arxiv.org/abs/1812.07811).

[71] A. Behring and W. Bizoń, “Higgs decay into massive b-quarks at NNLO QCD in the nested soft-collinear subtraction scheme,” *JHEP* **01** (2020) 189, [arXiv:1911.11524 \[hep-ph\]](https://arxiv.org/abs/1911.11524).

[72] G. Somogyi and F. Tramontano, “Fully exclusive heavy quark-antiquark pair production from a colourless initial state at NNLO in QCD,” *JHEP* **11** (2020) 142, [arXiv:2007.15015 \[hep-ph\]](https://arxiv.org/abs/2007.15015).

[73] J. Wang, X. Wang, and Y. Wang, “Analytic decay width of the Higgs boson to massive bottom quarks at order  $\alpha_s^3$ ,” *JHEP* **03** (2025) 163, [arXiv:2411.07493 \[hep-ph\]](https://arxiv.org/abs/2411.07493).

[74] F. Herzog, B. Ruijl, T. Ueda, J. A. M. Vermaseren, and A. Vogt, “On Higgs decays to hadrons and the R-ratio at  $N^4LO$ ,” *JHEP* **08** (2017) 113, [arXiv:1707.01044 \[hep-ph\]](https://arxiv.org/abs/1707.01044).

[75] R. Mondini, M. Schiavi, and C. Williams, “ $N^3LO$  predictions for the decay of the Higgs boson to bottom quarks,” *JHEP* **06** (2019) 079, [arXiv:1904.08960 \[hep-ph\]](https://arxiv.org/abs/1904.08960).

[76] X. Chen, P. Jakubčík, M. Marcoli, and G. Stagnitto, “The parton-level structure of Higgs decays to hadrons at  $N^3LO$ ,” *JHEP* **06** (2023) 185, [arXiv:2304.11180 \[hep-ph\]](https://arxiv.org/abs/2304.11180).

[77] J. Wang, Y. Wang, and D.-J. Zhang, “Analytic decay width of the Higgs boson to massive bottom quarks at next-to-next-to-leading order in QCD,” *JHEP* **03** (2024) 068, [arXiv:2310.20514 \[hep-ph\]](https://arxiv.org/abs/2310.20514).

[78] K. G. Chetyrkin, B. A. Kniehl, and M. Steinhauser, “Virtual top quark effects on the  $H \rightarrow b\bar{b}$  decay at next-to-leading order in QCD,” *Phys. Rev. Lett.* **78** (1997) 594–597, [arXiv:hep-ph/9610456](https://arxiv.org/abs/hep-ph/9610456).

[79] A. Kwiatkowski and M. Steinhauser, “Corrections of order  $\mathcal{O}(G_F \alpha_s m_t^2)$  to the Higgs decay rate  $\Gamma(H \rightarrow b\bar{b})$ ,” *Phys. Lett. B* **338** (1994) 66–70, [arXiv:hep-ph/9405308](https://arxiv.org/abs/hep-ph/9405308). [Erratum: *Phys. Lett. B* 342, 455–455 (1995)].

[80] B. A. Kniehl and M. Spira, “Two loop  $\mathcal{O}(\alpha_s G_F m_t^2)$  correction to the  $H \rightarrow b\bar{b}$  decay rate,” *Nucl. Phys. B* **432** (1994) 39–48, [arXiv:hep-ph/9410319](https://arxiv.org/abs/hep-ph/9410319).

[81] A. L. Kataev, “The  $\mathcal{O}(\alpha \alpha_s)$  and  $\mathcal{O}(\alpha^2)$  corrections to the decay width of the neutral Higgs boson to the  $b\bar{b}$  pair,” *JETP Lett.* **66** (1997) 327–330, [arXiv:hep-ph/9708292](https://arxiv.org/abs/hep-ph/9708292).

[82] A. Djouadi, P. Gambino, and B. A. Kniehl, “Two loop electroweak heavy fermion corrections to Higgs boson production and decay,” *Nucl. Phys. B* **523** (1998) 17–39, [arXiv:hep-ph/9712330](https://arxiv.org/abs/hep-ph/9712330).

[83] L. Mihaila, B. Schmidt, and M. Steinhauser, “ $\Gamma(H \rightarrow b\bar{b})$  to order  $\alpha \alpha_s$ ,” *Phys. Lett. B* **751** (2015) 442–447, [arXiv:1509.02294 \[hep-ph\]](https://arxiv.org/abs/1509.02294).

[84] J. Alwall, R. Frederix, S. Frixione, V. Hirschi, F. Maltoni, O. Mattelaer, H. S. Shao, T. Stelzer, P. Torrielli, and M. Zaro, “The automated computation of tree-level and

next-to-leading order differential cross sections, and their matching to parton shower simulations,” *JHEP* **07** (2014) 079, [arXiv:1405.0301 \[hep-ph\]](https://arxiv.org/abs/1405.0301).

- [85] K. G. Chetyrkin, J. H. Kuhn, and M. Steinhauser, “RunDec: A Mathematica package for running and decoupling of the strong coupling and quark masses,” *Comput. Phys. Commun.* **133** (2000) 43–65, [arXiv:hep-ph/0004189](https://arxiv.org/abs/hep-ph/0004189).
- [86] F. Herren and M. Steinhauser, “Version 3 of RunDec and CRunDec,” *Comput. Phys. Commun.* **224** (2018) 333–345, [arXiv:1703.03751 \[hep-ph\]](https://arxiv.org/abs/1703.03751).
- [87] A. Celis, J. Fuentes-Martin, A. Vicente, and J. Virto, “DsixTools: The Standard Model Effective Field Theory Toolkit,” *Eur. Phys. J. C* **77** no. 6, (2017) 405, [arXiv:1704.04504 \[hep-ph\]](https://arxiv.org/abs/1704.04504).
- [88] J. Fuentes-Martin, P. Ruiz-Femenia, A. Vicente, and J. Virto, “DsixTools 2.0: The Effective Field Theory Toolkit,” *Eur. Phys. J. C* **81** no. 2, (2021) 167, [arXiv:2010.16341 \[hep-ph\]](https://arxiv.org/abs/2010.16341).
- [89] S. Actis, G. Passarino, C. Sturm, and S. Uccirati, “NNLO Computational Techniques: The Cases  $H \rightarrow \gamma\gamma$  and  $H \rightarrow gg$ ,” *Nucl. Phys. B* **811** (2009) 182–273, [arXiv:0809.3667 \[hep-ph\]](https://arxiv.org/abs/0809.3667).
- [90] G. Degrassi and F. Maltoni, “Two-loop electroweak corrections to the Higgs-boson decay  $H \rightarrow \gamma\gamma$ ,” *Nucl. Phys. B* **724** (2005) 183–196, [arXiv:hep-ph/0504137](https://arxiv.org/abs/hep-ph/0504137).
- [91] G. Passarino, C. Sturm, and S. Uccirati, “Complete Two-Loop Corrections to  $H \rightarrow \gamma\gamma$ ,” *Phys. Lett. B* **655** (2007) 298–306, [arXiv:0707.1401 \[hep-ph\]](https://arxiv.org/abs/0707.1401).
- [92] P. Maierhöfer and P. Marquard, “Complete three-loop QCD corrections to the decay  $H \rightarrow \gamma\gamma$ ,” *Phys. Lett. B* **721** (2013) 131–135, [arXiv:1212.6233 \[hep-ph\]](https://arxiv.org/abs/1212.6233).
- [93] M. Niggetiedt, “Exact quark-mass dependence of the Higgs-photon form factor at three loops in QCD,” *JHEP* **04** (2021) 196, [arXiv:2009.10556 \[hep-ph\]](https://arxiv.org/abs/2009.10556).
- [94] J. Davies and F. Herren, “Higgs boson decay into photons at four loops,” *Phys. Rev. D* **104** no. 5, (2021) 053010, [arXiv:2104.12780 \[hep-ph\]](https://arxiv.org/abs/2104.12780).
- [95] Z.-Q. Chen, L.-B. Chen, C.-F. Qiao, and R. Zhu, “Two-loop electroweak corrections to the Higgs boson rare decay process  $H \rightarrow Z\gamma$ ,” *Phys. Rev. D* **110** no. 5, (2024) L051301, [arXiv:2404.11441 \[hep-ph\]](https://arxiv.org/abs/2404.11441).
- [96] W.-L. Sang, F. Feng, and Y. Jia, “Next-to-leading-order electroweak correction to  $H \rightarrow Z0\gamma$ ,” *Phys. Rev. D* **110** no. 5, (2024) L051302, [arXiv:2405.03464 \[hep-ph\]](https://arxiv.org/abs/2405.03464).
- [97] T. Gehrmann, S. Guns, and D. Kara, “The rare decay  $H \rightarrow Z\gamma$  in perturbative QCD,” *JHEP* **09** (2015) 038, [arXiv:1505.00561 \[hep-ph\]](https://arxiv.org/abs/1505.00561).
- [98] R. Bonciani, V. Del Duca, H. Frellesvig, J. M. Henn, F. Moriello, and V. A. Smirnov, “Next-to-leading order QCD corrections to the decay width  $H \rightarrow Z\gamma$ ,” *JHEP* **08** (2015) 108, [arXiv:1505.00567 \[hep-ph\]](https://arxiv.org/abs/1505.00567).
- [99] M. Spira, A. Djouadi, and P. Zerwas, “Qcd corrections to the  $hZ\gamma$  coupling,” *Physics Letters B* **276** no. 3, (1992) 350–353.  
<https://www.sciencedirect.com/science/article/pii/037026939290331W>.
- [100] A. Abbasabadi and W. W. Repko, “Higgs boson decay into two gluons and a Z boson,” *Int. J. Theor. Phys.* **47** (2008) 1490–1496.
- [101] B. A. Kniehl, “The Higgs Boson Decay  $H \rightarrow Z gg$ ,” *Phys. Lett. B* **244** (1990) 537–540.

[102] A. Rossia, M. Thomas, and E. Vryonidou, “Diboson production in the SMEFT from gluon fusion,” *JHEP* **11** (2023) 132, [arXiv:2306.09963 \[hep-ph\]](https://arxiv.org/abs/2306.09963).

[103] L. Bellafronte, G. Degrassi, P. P. Giardino, R. Gröber, and M. Vitti, “Gluon fusion production at NLO: merging the transverse momentum and the high-energy expansions,” *JHEP* **07** (2022) 069, [arXiv:2202.12157 \[hep-ph\]](https://arxiv.org/abs/2202.12157).

[104] **ATLAS** Collaboration, G. Aad *et al.*, “Measurement of the  $H \rightarrow \gamma\gamma$  and  $H \rightarrow ZZ^* \rightarrow 4\ell$  cross-sections in pp collisions at  $\sqrt{s} = 13.6$  TeV with the ATLAS detector,” *Eur. Phys. J. C* **84** no. 1, (2024) 78, [arXiv:2306.11379 \[hep-ex\]](https://arxiv.org/abs/2306.11379).

[105] **CMS** Collaboration, V. Chekhovsky *et al.*, “Measurements of the Higgs boson production cross section in the four-lepton final state in proton-proton collisions at  $\sqrt{s} = 13.6$  TeV,” *JHEP* **05** (2025) 079, [arXiv:2501.14849 \[hep-ex\]](https://arxiv.org/abs/2501.14849).

[106] G. Degrassi, P. P. Giardino, F. Maltoni, and D. Pagani, “Probing the Higgs self coupling via single Higgs production at the LHC,” *JHEP* **12** (2016) 080, [arXiv:1607.04251 \[hep-ph\]](https://arxiv.org/abs/1607.04251).

[107] G. Degrassi, M. Fedele, and P. P. Giardino, “Constraints on the trilinear Higgs self coupling from precision observables,” *JHEP* **04** (2017) 155, [arXiv:1702.01737 \[hep-ph\]](https://arxiv.org/abs/1702.01737).

[108] M. Gorbahn and U. Haisch, “Indirect probes of the trilinear Higgs coupling:  $gg \rightarrow h$  and  $h \rightarrow \gamma\gamma$ ,” *JHEP* **10** (2016) 094, [arXiv:1607.03773 \[hep-ph\]](https://arxiv.org/abs/1607.03773).

[109] V. Maura, B. A. Stefanek, and T. You, “The Higgs Self-Coupling at FCC-ee,” [arXiv:2503.13719 \[hep-ph\]](https://arxiv.org/abs/2503.13719).

[110] J. ter Hoeve, L. Mantani, J. Rojo, A. N. Rossia, and E. Vryonidou, “Higgs trilinear coupling in the standard model effective field theory at the high luminosity LHC and the FCC-ee,” *Phys. Rev. D* **112** no. 1, (2025) 013008, [arXiv:2504.05974 \[hep-ph\]](https://arxiv.org/abs/2504.05974).

[111] S. Di Vita, C. Grojean, G. Panico, M. Riembau, and T. Vantalon, “A global view on the Higgs self-coupling,” *JHEP* **09** (2017) 069, [arXiv:1704.01953 \[hep-ph\]](https://arxiv.org/abs/1704.01953).

[112] **ATLAS** Collaboration, “Projections for measurements of Higgs boson cross sections, branching ratios, coupling parameters and mass with the ATLAS detector at the HL-LHC,” tech. rep., CERN, Geneva, 2018. <https://cds.cern.ch/record/2652762>. All figures including auxiliary figures are available at <https://atlas.web.cern.ch/Atlas/GROUPS/PHYSICS/PUBNOTES/ATL-PHYS-PUB-2018-054>.

[113] ATLAS and C. Collaborations, “Highlights of the hl-lhc physics projections by atlas and cms.” 2025. <https://arxiv.org/abs/2504.00672>.

[114] de Blas et. al., “Physics Briefing Book: Input for the 2026 update of the European Strategy for Particle Physics,” tech. rep., Geneva, 2025. <https://cds.cern.ch/record/2944678>.

[115] M. McCullough, “An Indirect Model-Dependent Probe of the Higgs Self-Coupling,” *Phys. Rev. D* **90** no. 1, (2014) 015001, [arXiv:1312.3322 \[hep-ph\]](https://arxiv.org/abs/1312.3322). [Erratum: Phys.Rev.D 92, 039903 (2015)].

[116] J. Altmann *et al.*, *ECFA Higgs, electroweak, and top Factory Study*, vol. 5/2025 of *CERN Yellow Reports: Monographs*. 6, 2025. [arXiv:2506.15390 \[hep-ex\]](https://arxiv.org/abs/2506.15390).

[117] A. Greljo, H. Tiblom, and A. Valenti, “New physics through flavor tagging at FCC-ee,” *SciPost Phys.* **18** no. 5, (2025) 152, [arXiv:2411.02485 \[hep-ph\]](https://arxiv.org/abs/2411.02485).

[118] S.-F. Ge, Z. Qian, M. J. Ramsey-Musolf, and J. Zhou, “New physics off the Z-pole:  $e^+e^- \rightarrow f\bar{f}$  at Future Lepton Colliders,” *JHEP* **06** (2025) 067, [arXiv:2410.17605 \[hep-ph\]](https://arxiv.org/abs/2410.17605).

[119] L. Bellafronte, S. Dawson, P. P. Giardino, and H. Liu, “Probing Top Quark-Electron Interactions at Future Colliders,” [arXiv:2507.02039 \[hep-ph\]](https://arxiv.org/abs/2507.02039).

[120] L. Allwicher, C. Grojean, and L. Tabatt, “Could electron-top interactions spoil the measurement of the Higgs trilinear? -A quantitative estimate at future lepton colliders-,” [arXiv:2512.06916 \[hep-ph\]](https://arxiv.org/abs/2512.06916).

[121] S. Dawson, S. Homiller, and S. D. Lane, “Putting standard model EFT fits to work,” *Phys. Rev. D* **102** no. 5, (2020) 055012, [arXiv:2007.01296 \[hep-ph\]](https://arxiv.org/abs/2007.01296).

[122] M. Gorbahn, J. M. No, and V. Sanz, “Benchmarks for Higgs Effective Theory: Extended Higgs Sectors,” *JHEP* **10** (2015) 036, [arXiv:1502.07352 \[hep-ph\]](https://arxiv.org/abs/1502.07352).

[123] T. Robens and T. Stefaniak, “LHC Benchmark Scenarios for the Real Higgs Singlet Extension of the Standard Model,” *Eur. Phys. J. C* **76** no. 5, (2016) 268, [arXiv:1601.07880 \[hep-ph\]](https://arxiv.org/abs/1601.07880).

[124] C.-Y. Chen, J. Kozaczuk, and I. M. Lewis, “Non-resonant Collider Signatures of a Singlet-Driven Electroweak Phase Transition,” *JHEP* **08** (2017) 096, [arXiv:1704.05844 \[hep-ph\]](https://arxiv.org/abs/1704.05844).

[125] M. Carena, Z. Liu, and Y. Wang, “Electroweak phase transition with spontaneous  $Z_2$ -breaking,” *JHEP* **08** (2020) 107, [arXiv:1911.10206 \[hep-ph\]](https://arxiv.org/abs/1911.10206).

[126] M. Jiang, N. Craig, Y.-Y. Li, and D. Sutherland, “Complete one-loop matching for a singlet scalar in the Standard Model EFT,” *JHEP* **02** (2019) 031, [arXiv:1811.08878 \[hep-ph\]](https://arxiv.org/abs/1811.08878). [Erratum: JHEP 01, 135 (2021)].

[127] U. Haisch, M. Ruhdorfer, E. Salvioni, E. Venturini, and A. Weiler, “Singlet night in Feynman-ville: one-loop matching of a real scalar,” *JHEP* **04** (2020) 164, [arXiv:2003.05936 \[hep-ph\]](https://arxiv.org/abs/2003.05936). [Erratum: JHEP 07, 066 (2020)].

[128] T. Hahn, “CUBA: A Library for multidimensional numerical integration,” *Comput. Phys. Commun.* **168** (2005) 78–95, [arXiv:hep-ph/0404043](https://arxiv.org/abs/hep-ph/0404043).

[129] J. Aebischer *et al.*, “WCxf: an exchange format for Wilson coefficients beyond the Standard Model,” *Comput. Phys. Commun.* **232** (2018) 71–83, [arXiv:1712.05298 \[hep-ph\]](https://arxiv.org/abs/1712.05298).

[130] **Particle Data Group Collaboration** Collaboration, S. Navas *et al.*, “Review of particle physics,” *Phys. Rev. D* **110** (Aug, 2024) 030001. <https://link.aps.org/doi/10.1103/PhysRevD.110.030001>.

[131] I. Dubovyk, A. Freitas, J. Gluza, T. Riemann, and J. Usovitsch, “Electroweak pseudo-observables and Z-boson form factors at two-loop accuracy,” *JHEP* **08** (2019) 113, [arXiv:1906.08815 \[hep-ph\]](https://arxiv.org/abs/1906.08815).

[132] A. Freitas, “Higher-order electroweak corrections to the partial widths and branching ratios of the Z boson,” *JHEP* **04** (2014) 070, [arXiv:1401.2447 \[hep-ph\]](https://arxiv.org/abs/1401.2447).

[133] I. Dubovyk, A. Freitas, J. Gluza, T. Riemann, and J. Usovitsch, “Complete electroweak two-loop corrections to Z boson production and decay,” *Phys. Lett. B* **783** (2018) 86–94, [arXiv:1804.10236 \[hep-ph\]](https://arxiv.org/abs/1804.10236).

- [134] M. Awramik, M. Czakon, and A. Freitas, “Electroweak two-loop corrections to the effective weak mixing angle,” *JHEP* **11** (2006) 048, [arXiv:hep-ph/0608099](https://arxiv.org/abs/hep-ph/0608099).
- [135] M. Awramik, M. Czakon, A. Freitas, and B. A. Kniehl, “Two-loop electroweak fermionic corrections to  $\sin^{*2} \theta^* b$  anti- $b$ (eff),” *Nucl. Phys. B* **813** (2009) 174–187, [arXiv:0811.1364 \[hep-ph\]](https://arxiv.org/abs/0811.1364).
- [136] **FCC** Collaboration, “Prospects in electroweak, Higgs and Top physics at FCC,” .
- [137] V. Maura, B. A. Stefanek, and T. You, “Accuracy complements energy: electroweak precision tests at Tera-Z,” *JHEP* **10** (2025) 022, [arXiv:2412.14241 \[hep-ph\]](https://arxiv.org/abs/2412.14241).

## A Code

To make our results more easily accessible and replicable, we have written a publicly available code NEWiSH  [31] (**N**LO **E**lectro**W**eak in the **S**MEFT for **H**iggs widths). NEWiSH is a fixed-order Fortran code that computes the partial widths for the two- and three- body decay channels presented in this work at NLO accuracy in the SMEFT consistently retaining contributions to  $\mathcal{O}(\frac{1}{16\pi^2\Lambda^2})$ . NEWiSH also implements the full  $h \rightarrow 4f$  processes at LO,  $\mathcal{O}(\frac{1}{\Lambda^2})$ .

NEWiSH relies on the following dependencies:

- [json-fortran](#)
- [COLLIER](#) [39] for evaluating loop integrals
- [CUBA](#) [128] for numerical integration

All processes have been validated using **MADGRAPH** [84] at NLO QCD and EW in the SM, as well at LO in the SMEFT for a number of coefficients using **SMEFTsim** [8].

We use the **WCxf** format [129] for Wilson coefficient inputs, though we should emphasize that while our coefficients are evaluated at the scale  $\mu = m_h$  the code does **not** perform the running between the  $\Lambda$  and  $\mu$  scales needed for matching to specific UV models. This must be done independently using, for example, **DsixTools** [87, 88].

For up-to-date details on installation and usage of NEWiSH, we refer to the READMEs on the GitLab page.

## B Numerical results for $h \rightarrow f\bar{f}$ and $h \rightarrow VV'$

For completeness, here we include numerical results for  $h \rightarrow f\bar{f}$  and  $h \rightarrow VV'$  using the numerical inputs in Sec. 2.3. All results here are also available as data files at our NEWiSH GitLab repository [31]. Additionally, for  $h \rightarrow q\bar{q}$  we include results for  $\overline{\text{MS}}$  quark masses as well.

### B.1 $h \rightarrow l^+l^-$

Using the inputs of Sec. 2.3,

$$\begin{aligned} \Gamma_{\text{LO}}(h \rightarrow \tau^+\tau^-) &= 0.259 \times 10^{-3} \text{ GeV} \\ &+ \left( \frac{1 \text{ TeV}}{\Lambda} \right)^2 \left( 0.0314C_{\phi\Box} - 0.00785C_{\phi D} - 3.08C_{e\phi}[33] + 0.0157C_{ll}[1221] \right. \\ &\quad \left. - 0.0157C_{\phi l}^{(3)}[11] - 0.0157C_{\phi l}^{(3)}[22] \right) \times 10^{-3} \text{ GeV} \end{aligned} \quad (\text{B.1})$$

$$\begin{aligned}
\delta\Gamma_{\text{NLO}}(h \rightarrow \tau^+ \tau^-) &= -2.58 \times 10^{-6} \text{ GeV} \\
&+ \left( \frac{1 \text{ TeV}}{\Lambda} \right)^2 \left( 0.374C_\phi + 2.41C_{\phi B} + 0.567C_{\phi \square} + 0.599C_{\phi D} + 1.06C_{\phi W} \right. \\
&+ 0.213C_{\phi WB} + 0.017C_{d\phi}[33] + 2.62C_{eB}[33] - 67C_{e\phi}[33] - 9.58C_{eW}[33] \\
&- 0.154C_{le}[3333] + 0.857C_{ledq}[3333] - 0.262C_{lequ}^{(1)}[3322] - 54.9C_{lequ}^{(1)}[3333] \\
&- 0.345C_{ll}[1122] - 0.201C_{ll}[1221] + 0.0428C_{lq}^{(3)}[1133] + 0.0428C_{lq}^{(3)}[2233] \\
&- 0.0584C_{\phi e}[33] - 0.016C_{\phi l}^{(1)}[11] - 0.016C_{\phi l}^{(1)}[22] + 0.067C_{\phi l}^{(1)}[33] \\
&- 0.0598C_{\phi l}^{(3)}[11] - 0.0598C_{\phi l}^{(3)}[22] + 0.28C_{\phi l}^{(3)}[33] - 0.0856C_{\phi q}^{(3)}[33] \\
&\left. - 0.00583C_{\phi ud}[33] - 0.711C_{u\phi}[33] \right) \times 10^{-6} \text{ GeV}
\end{aligned} \tag{B.2}$$

where we have dropped terms contributing less than  $10^{-9}$  GeV. Note the change from  $10^{-3}$  to  $10^{-6}$  GeV in the NLO correction for ease of presentation.

For  $h \rightarrow \mu^+ \mu^-$ ,

$$\begin{aligned}
\Gamma_{\text{LO}}(h \rightarrow \mu^+ \mu^-) &= 0.917 \times 10^{-6} \text{ GeV} \\
&+ \left( \frac{1 \text{ TeV}}{\Lambda} \right)^2 \left( 0.111C_{\phi \square} - 0.0278C_{\phi D} - 183C_{e\phi}[22] \right. \\
&\left. + 0.0556C_{ll}[1221] - 0.0556C_{\phi l}^{(3)}[11] - 0.0556C_{\phi l}^{(3)}[22] \right) \times 10^{-6} \text{ GeV}
\end{aligned} \tag{B.3}$$

$$\begin{aligned}
\delta\Gamma_{\text{NLO}}(h \rightarrow \mu^+ \mu^-) &= -0.0278 \times 10^{-6} \text{ GeV} \\
&+ \left( \frac{1 \text{ TeV}}{\Lambda} \right)^2 \left( 0.00133C_\phi + 0.0204C_{\phi B} + 0.00467C_{\phi D} + 0.00721C_{\phi W} \right. \\
&- 0.00179C_{\phi WB} + 0.157C_{eB}[22] - 2.11C_{e\phi}[22] - 0.571C_{eW}[22] \\
&- 0.00919C_{le}[2332] + 0.00103C_{ledq}[2222] + 0.051C_{ledq}[2233] \\
&- 0.0156C_{lequ}^{(1)}[2222] - 3.27C_{lequ}^{(1)}[2233] - 0.00122C_{ll}[1122] \\
&- 0.00298C_{ll}[1221] + 0.00206C_{\phi l}^{(3)}[11] + 0.00305C_{\phi l}^{(3)}[22] \\
&\left. - 0.00252C_{u\phi}[33] \right) \times 10^{-6} \text{ GeV}
\end{aligned} \tag{B.4}$$

where we have dropped contributions smaller than  $10^{-9}$  GeV.

## B.2 $h \rightarrow q\bar{q}$

### B.2.1 On-shell inputs

With the inputs of Sec. 2.3 and using OS renormalization for the fermion masses,

$$\begin{aligned} \Gamma_{\text{LO}}(h \rightarrow b\bar{b}) &= 5.91 \times 10^{-3} \text{ GeV} \\ &+ \left( \frac{1 \text{ TeV}}{\Lambda} \right)^2 \left( 0.716C_{\phi\Box} - 0.179C_{\phi D} - 25.3C_{d\phi}[33] + 0.358C_{ll}[1221] \right. \\ &\left. - 0.358C_{\phi l}^{(3)}[11] - 0.358C_{\phi l}^{(3)}[22] \right) \times 10^{-3} \text{ GeV} \end{aligned} \quad (\text{B.5})$$

$$\begin{aligned} \delta\Gamma_{\text{NLO}}(h \rightarrow b\bar{b}) &= -2.25 \times 10^{-3} \text{ GeV} \\ &+ \left( \frac{1 \text{ TeV}}{\Lambda} \right)^2 \left( 0.00847C_{\phi} + 0.00274C_{\phi B} - 0.253C_{\phi\Box} + 0.0653C_{\phi D} \right. \\ &+ 0.922C_{\phi G} + 0.0097C_{\phi W} + 0.00105C_{\phi WB} + 0.00211C_{dB}[33] - 0.132C_{dG}[33] \\ &+ 1.47C_{d\phi}[33] + 1.01C_{dW}[33] + 0.0000463C_{e\phi}[33] + 0.000847C_{ledq}[3333] \\ &- 0.00788C_{ll}[1122] - 0.138C_{ll}[1221] - 1.89 \times 10^{-6}C_{ll}[1331] \\ &- 1.89 \times 10^{-6}C_{ll}[2332] + 0.000976C_{lq}^{(3)}[1133] + 0.000976C_{lq}^{(3)}[2233] \\ &- 0.000717C_{\phi d}[33] - 0.000366C_{\phi l}^{(1)}[11] - 0.000366C_{\phi l}^{(1)}[22] + 0.132C_{\phi l}^{(3)}[11] \\ &+ 0.132C_{\phi l}^{(3)}[22] + 4.26 \times 10^{-6}C_{\phi l}^{(3)}[33] + 0.00212C_{\phi q}^{(1)}[33] - 0.0109C_{\phi q}^{(3)}[33] \\ &- 0.0631C_{\phi ud}[33] - 0.00354C_{qd}^{(1)}[3333] - 0.00473C_{qd}^{(8)}[3333] + 0.528C_{quqd}^{(1)}[3333] \\ &\left. + 0.101C_{quqd}^{(8)}[3333] - 0.0108C_{u\phi}[33] + 0.0164C_{uW}[33] \right) \times 10^{-3} \text{ GeV} \end{aligned} \quad (\text{B.6})$$

where we have not dropped any contributions.

For  $h \rightarrow c\bar{c}$ ,

$$\begin{aligned} \Gamma_{\text{LO}}(h \rightarrow c\bar{c}) &= 0.561 \times 10^{-3} \text{ GeV} \\ &+ \left( \frac{1 \text{ TeV}}{\Lambda} \right)^2 \left( 0.068C_{\phi\Box} - 0.017C_{\phi D} + 0.034C_{ll}[1221] - 0.034C_{\phi l}^{(3)}[11] \right. \\ &\left. - 0.034C_{\phi l}^{(3)}[22] - 7.84C_{u\phi}[22] \right) \times 10^{-3} \text{ GeV} \end{aligned} \quad (\text{B.7})$$

$$\begin{aligned}
\delta\Gamma_{\text{NLO}}(h \rightarrow c\bar{c}) = & -0.309 \times 10^{-3} \text{ GeV} \\
& + \left( \frac{1 \text{ TeV}}{\Lambda} \right)^2 \left( 0.00081C_\phi + 0.00234C_{\phi B} - 0.0356C_{\phi\Box} + 0.00966C_{\phi D} \right. \\
& + 0.15C_{\phi G} + 0.0016C_{\phi W} + 0.000153C_{\phi WB} + 0.0000369C_{d\phi}[33] \\
& + 4.4 \times 10^{-6}C_{e\phi}[33] - 0.000262C_{lequ}^{(1)}[3322] - 0.000749C_{ll}[1122] \\
& - 0.0184C_{ll}[1221] + 0.0000927C_{lq}^{(3)}[1133] + 0.0000927C_{lq}^{(3)}[2233] \\
& - 0.0000347C_{\phi l}^{(1)}[11] - 0.0000347C_{\phi l}^{(1)}[22] + 0.0178C_{\phi l}^{(3)}[11] + 0.0178C_{\phi l}^{(3)}[22] \\
& - 0.000174C_{\phi q}^{(1)}[22] + 0.000634C_{\phi q}^{(3)}[22] - 0.000185C_{\phi q}^{(3)}[33] + 0.0000983C_{\phi u}[22] \\
& - 0.0000126C_{\phi ud}[33] - 0.000334C_{qu}^{(1)}[2222] - 0.178C_{qu}^{(1)}[2332] \\
& - 0.000446C_{qu}^{(8)}[2222] - 0.237C_{qu}^{(8)}[2332] + 0.00219C_{quqd}^{(1)}[2233] \\
& + 0.000364C_{quqd}^{(1)}[3223] + 0.000486C_{quqd}^{(8)}[3223] - 0.0037C_{uB}[22] \\
& - 0.0416C_{uG}[22] + 1.13C_{u\phi}[22] - 0.00154C_{u\phi}[33] \\
& \left. - 0.0245C_{uW}[22] \right) \times 10^{-3} \text{ GeV}
\end{aligned} \tag{B.8}$$

where we have dropped terms contributing less than  $10^{-9}$  GeV.

For  $h \rightarrow s\bar{s}$

$$\begin{aligned}
\Gamma_{\text{LO}}(h \rightarrow s\bar{s}) = & 2.46 \times 10^{-6} \text{ GeV} \\
& + \left( \frac{1 \text{ TeV}}{\Lambda} \right)^2 \left( 0.299C_{\phi\Box} - 0.0747C_{\phi D} - 520C_{d\phi}[22] + 0.149C_{ll}[1221] \right. \\
& \left. - 0.149C_{\phi l}^{(3)}[11] - 0.149C_{\phi l}^{(3)}[22] \right) \times 10^{-6} \text{ GeV}
\end{aligned} \tag{B.9}$$

$$\begin{aligned}
\delta\Gamma_{\text{NLO}}(h \rightarrow s\bar{s}) = & -2.35 \times 10^{-6} \text{ GeV} \\
& + \left( \frac{1 \text{ TeV}}{\Lambda} \right)^2 \left( 0.00356C_\phi + 0.00533C_{\phi B} - 0.277C_{\phi\Box} + 0.0709C_{\phi D} \right. \\
& + 1.47C_{\phi G} + 0.00581C_{\phi W} + 0.0474C_{dB}[22] - 2.77C_{dG}[22] + 181.C_{d\phi}[22] \\
& - 1.62C_{dW}[22] + 0.00103C_{ledq}[2222] + 0.0174C_{ledq}[3322] - 0.00329C_{ll}[1122] \\
& - 0.14C_{ll}[1221] + 0.138C_{\phi l}^{(3)}[11] + 0.138C_{\phi l}^{(3)}[22] + 0.00289C_{\phi q}^{(3)}[22] \\
& - 0.00329C_{\phi ud}[22] - 0.00146C_{qd}^{(1)}[2222] - 0.0727C_{qd}^{(1)}[2332] - 0.00195C_{qd}^{(8)}[2222] \\
& - 0.097C_{qd}^{(8)}[2332] + 0.0517C_{quqd}^{(1)}[2222] + 1.55C_{quqd}^{(1)}[2332] + 9.28C_{quqd}^{(1)}[3322] \\
& \left. + 0.00984C_{quqd}^{(8)}[2222] + 2.06C_{quqd}^{(8)}[2332] - 0.00676C_{u\phi}[33] \right) \times 10^{-6} \text{ GeV}
\end{aligned} \tag{B.10}$$

where we have dropped terms smaller than  $10^{-9}$  GeV.

### B.2.2 $\overline{\text{MS}}$ inputs

As discussed in Sec. 3.3.1, the choice of  $\overline{\text{MS}}$  inputs for the quark masses makes a significant difference for the  $h \rightarrow q\bar{q}$  processes. Here we give the expressions for the  $\overline{\text{MS}}$  inputs in Sec. 2.3 while keeping all other inputs the same. This contribution is also implemented in NEWiSH for these fixed inputs. Note that for each of  $b\bar{b}$ ,  $c\bar{c}$ , and  $s\bar{s}$  there are numerous small contributions introduced in this scheme from the running of the quark mass from  $\mu = m_q$  to  $\mu = m_h$  which we neglect here for brevity.

For  $h \rightarrow b\bar{b}$  we have

$$\begin{aligned} \Gamma_{\text{LO}}^{\overline{\text{MS}}}(h \rightarrow b\bar{b}) &= 6.58 \times 10^{-3} \text{ GeV} \\ &+ \left( \frac{1 \text{ TeV}}{\Lambda} \right)^2 \left( 0.798C_{\phi\Box} - 0.199C_{\phi D} - 26.7C_{d\phi}[33] + 0.399C_{ll}[1221] \right. \\ &\quad \left. - 0.399C_{\phi l}^{(3)}[11] - 0.399C_{\phi l}^{(3)}[22] \right) \times 10^{-3} \text{ GeV} \end{aligned} \quad (\text{B.11})$$

$$\begin{aligned} \delta\Gamma_{\text{NLO}}^{\overline{\text{MS}}}(h \rightarrow b\bar{b}) &= -2.45 \times 10^{-3} \text{ GeV} \\ &+ \left( \frac{1 \text{ TeV}}{\Lambda} \right)^2 \left( -0.00103C_G + 0.00942C_\phi + 0.00294C_{\phi B} - 0.275C_{\phi\Box} + 0.0701C_{\phi D} \right. \\ &\quad + 1.C_{\phi G} + 0.0113C_{\phi W} + 0.0388C_{dB}[33] + 0.0994C_{dG}[33] + 1.24C_{d\phi}[33] + 1.8C_{dW}[33] \\ &\quad - 0.00878C_{ll}[1122] - 0.15C_{ll}[1221] + 0.00118C_{lq}^{(3)}[1133] + 0.00118C_{lq}^{(3)}[2233] \\ &\quad - 0.00317C_{\phi d}[33] + 0.144C_{\phi l}^{(3)}[11] + 0.144C_{\phi l}^{(3)}[22] + 0.00273C_{\phi q}^{(1)}[33] - 0.023C_{\phi q}^{(3)}[33] \\ &\quad - 0.0363C_{\phi ud}[33] - 0.00218C_{qd}^{(1)}[3333] - 0.00231C_{qd}^{(8)}[3333] + 0.00184C_{qq}^{(1)}[3333] \\ &\quad - 0.00882C_{qq}^{(3)}[3333] + 0.00119C_{qu}^{(1)}[3333] + 0.00262C_{qu}^{(8)}[3333] - 0.00108C_{quqd}^{(1)}[2233] \\ &\quad + 2.76C_{quqd}^{(1)}[3333] + 0.389C_{quqd}^{(8)}[3333] + 0.00428C_{uG}[33] - 0.0119C_{u\phi}[33] \\ &\quad \left. + 0.0258C_{uW}[33] \right) \times 10^{-3} \text{ GeV} \end{aligned} \quad (\text{B.12})$$

where we have truncated at  $10^{-6}$  GeV.

For  $h \rightarrow c\bar{c}$ , we find

$$\begin{aligned} \Gamma_{\text{LO}}^{\overline{\text{MS}}}(h \rightarrow c\bar{c}) &= 2.28 \times 10^{-3} \text{ GeV} \\ &+ \left( \frac{1 \text{ TeV}}{\Lambda} \right)^2 \left( 2.28 + 0.277C_{\phi\Box} - 0.0691C_{\phi D} + 0.138C_{ll}[1221] \right. \\ &\quad \left. - 0.138C_{\phi l}^{(3)}[11] - 0.138C_{\phi l}^{(3)}[22] - 15.8C_{u\phi}[22] \right) \times 10^{-3} \text{ GeV} \end{aligned} \quad (\text{B.13})$$

$$\begin{aligned}
\delta\Gamma_{\text{NLO}}^{\overline{\text{MS}}}(h \rightarrow c\bar{c}) &= -1.01 \times 10^{-3} \text{ GeV} \\
&+ \left( \frac{1 \text{ TeV}}{\Lambda} \right)^2 \left( 0.00328C_\phi + 0.00695C_{\phi B} - 0.114C_{\phi\Box} + 0.0309C_{\phi D} + 0.45C_{\phi G} \right. \\
&+ 0.00579C_{\phi W} - 0.00309C_{ll}[1122] - 0.0587C_{ll}[1221] + 0.0565C_{\phi l}^{(3)}[11] \\
&+ 0.0565C_{\phi l}^{(3)}[22] + 0.00296C_{\phi q}^{(3)}[22] - 0.00165C_{qq}^{(3)}[2233] - 1.42C_{qu}^{(1)}[2332] \\
&- 1.98C_{qu}^{(8)}[2332] - 0.0186C_{uB}[22] - 0.0918C_{uG}[22] + 1.24C_{u\phi}[22] \\
&\left. - 0.00617C_{u\phi}[33] + 0.0544C_{uW}[22] \right) \times 10^{-3} \text{ GeV}
\end{aligned} \tag{B.14}$$

where we have truncated at  $10^{-6}$ .

Finally for  $h \rightarrow s\bar{s}$  we find

$$\begin{aligned}
\Gamma_{\text{LO}}^{\overline{\text{MS}}}(h \rightarrow s\bar{s}) &= 10 \times 10^{-6} \text{ GeV} \\
&+ \left( \frac{1 \text{ TeV}}{\Lambda} \right)^2 \left( 1.22C_{\phi\Box} - 0.304C_{\phi D} - 1050.C_{d\phi}[22] + 0.608C_{ll}[1221] \right. \\
&\left. - 0.608C_{\phi l}^{(3)}[11] - 0.608C_{\phi l}^{(3)}[22] \right) \times 10^{-6} \text{ GeV}
\end{aligned} \tag{B.15}$$

$$\begin{aligned}
\delta\Gamma_{\text{NLO}}^{\overline{\text{MS}}}(h \rightarrow s\bar{s}) &= -8.49 \times 10^{-6} \text{ GeV} \\
&+ \left( \frac{1 \text{ TeV}}{\Lambda} \right)^2 \left( 0.0145C_\phi + 0.0194C_{\phi B} - 0.995C_{\phi\Box} + 0.254C_{\phi D} + 5.2C_{\phi G} \right. \\
&+ 0.0229C_{\phi W} + 1.25C_{dB}[22] - 2.77C_{dG}[22] + 298.C_{d\phi}[22] + 4.19C_{dW}[22] \\
&- 0.00895C_{ledq}[3322] - 0.0137C_{ll}[1122] - 0.498C_{ll}[1221] - 0.00462C_{\phi d}[22] \\
&+ 0.489C_{\phi l}^{(3)}[11] + 0.489C_{\phi l}^{(3)}[22] + 0.00862C_{\phi q}^{(1)}[22] + 0.0176C_{\phi q}^{(3)}[22] \\
&- 0.00384C_{\phi q}^{(3)}[33] - 0.0436C_{\phi ud}[22] - 0.00239C_{qd}^{(1)}[2222] - 0.0348C_{qd}^{(1)}[2332] \\
&- 0.00335C_{qd}^{(8)}[2222] - 0.0445C_{qd}^{(8)}[2332] - 0.0062C_{qq}^{(3)}[2233] - 0.00244C_{qq}^{(3)}[2332] \\
&+ 0.00292C_{qu}^{(1)}[3333] + 0.00383C_{qu}^{(8)}[3333] + 0.134C_{quqd}^{(1)}[2222] + 45.1C_{quqd}^{(1)}[2332] \\
&+ 114.C_{quqd}^{(1)}[3322] + 0.0278C_{quqd}^{(8)}[2222] + 19.1C_{quqd}^{(8)}[2332] + 1.17C_{quqd}^{(8)}[3322] \\
&\left. + 0.00163C_{uG}[33] - 0.0271C_{u\phi}[33] \right) \times 10^{-6} \text{ GeV}
\end{aligned} \tag{B.16}$$

where we have truncated at  $10^{-9}$  GeV.

### B.3 $h \rightarrow \gamma\gamma$

With the inputs of Sec. 2.3,

$$\Gamma_{\text{LO}}(h \rightarrow \gamma\gamma) = \left( \frac{1 \text{ TeV}}{\Lambda} \right)^2 (-0.243C_{\phi B} - 0.0697C_{\phi W} + 0.130C_{\phi WB}) \times 10^{-3} \text{ GeV} \tag{B.17}$$

$$\begin{aligned}
\delta\Gamma_{\text{NLO}}(h \rightarrow \gamma\gamma) &= 9.80 \times 10^{-6} \text{ GeV} \\
&+ \left( \frac{1 \text{ TeV}}{\Lambda} \right)^2 \left( 8.93C_{\phi B} + 0.594C_{\phi\square} - 1.18C_{\phi D} - 1.20C_{\phi W} \right. \\
&- 1.96C_{\phi WB} - 0.167C_W + 1.78C_{ll}[1221] - 1.78C_{\phi l}^{(3)}[11] - 1.78C_{\phi l}^{(3)}[22] \\
&\left. + 6.74C_{uB}[33] + 0.169C_{u\phi}[33] + 3.61C_{uW}[33] \right) \times 10^{-6} \text{ GeV}
\end{aligned} \tag{B.18}$$

#### B.4 $h \rightarrow \gamma Z$

With the inputs of Sec. 2.3 and taking all fermions massless except for  $m_t$ ,

$$\Gamma_{\text{LO}}(h \rightarrow \gamma Z) = \left( \frac{1 \text{ TeV}}{\Lambda} \right)^2 (0.0476C_{\phi B} - 0.0476C_{\phi W} + 0.0317C_{\phi WB}) \times 10^{-3} \text{ GeV.} \tag{B.19}$$

$$\begin{aligned}
\delta\Gamma_{\text{NLO}}(h \rightarrow \gamma Z) &= 6.52 \times 10^{-6} \text{ GeV} \\
&+ \left( \frac{1 \text{ TeV}}{\Lambda} \right)^2 \left( 0.391C_{\phi B} + 0.395C_{\phi\square} - 0.392C_{\phi D} - 0.61C_{\phi W} \right. \\
&- 1.59C_{\phi WB} - 0.246C_W + 1.19C_{ll}[1221] - 1.19C_{\phi l}^{(3)}[11] - 1.19C_{\phi l}^{(3)}[22] \\
&+ 0.0576C_{\phi q}^{(1)}[33] - 0.0576C_{\phi q}^{(3)}[33] + 0.0576C_{\phi u}[33] - 0.228C_{uB}[33] \\
&\left. + 0.0235C_{u\phi}[33] + 1.50C_{uW}[33] \right) \times 10^{-6} \text{ GeV.}
\end{aligned} \tag{B.20}$$

#### B.5 $h \rightarrow gg$

With the inputs of Sec. 2.3 and the assumptions discussed in Sec. 3.4,

$$\Gamma_{\text{LO}}(h \rightarrow gg) = 7.60C_{\phi G} \left( \frac{1 \text{ TeV}}{\Lambda} \right)^2 \times 10^{-3} \text{ GeV} \tag{B.21}$$

$$\begin{aligned}
\delta\Gamma_{\text{NLO}}(h \rightarrow gg) &= 0.193 \times 10^{-3} \text{ GeV} \\
&+ \left( \frac{1 \text{ TeV}}{\Lambda} \right)^2 \left( 0.0234C_{\phi\square} - 0.00585C_{\phi D} + 0.0130C_{dG}[33] \right. \\
&+ 0.0469C_{d\phi}[33] + 0.0117C_{ll}[1221] - 0.0117C_{\phi l}^{(3)}[11] - 0.0117C_{\phi l}^{(3)}[22] \\
&\left. - 0.189C_{uG}[33] - 0.0249C_{u\phi}[33] \right) \times 10^{-3} \text{ GeV.}
\end{aligned} \tag{B.22}$$

## C Projected Sensitivities at Tera-Z

We report here the numerical values used for the observables entering the results presented in this work. The current values of the electroweak precision observables used in Sec. 4.1 are summarized in Tab. 1. The experimental values are taken from Tab. 10.3 of the Particle

Measurement	Current Experiment	Current theory
$\Gamma_Z(\text{GeV})$	$2.4955 \pm 0.0023$	$2.4943 \pm 0.0006$ [131–133]
$R_e$	$20.804 \pm 0.05$	$20.732 \pm 0.009$ [131–133]
$R_\mu$	$20.784 \pm 0.034$	$20.732 \pm 0.009$ [131–133]
$R_\tau$	$20.764 \pm 0.045$	$20.779 \pm 0.009$ [131–133]
$R_b$	$0.21629 \pm 0.00066$	$0.2159 \pm 0.0001$ [131–133]
$R_c$	$0.1721 \pm 0.0030$	$0.1722 \pm 0.00005$ [131–133]
$\sigma_h$	$41.4802 \pm 0.0325$	$41.492 \pm 0.008$ [131–133]
$A_e$ (from $A_{LR}$ had)	$0.15138 \pm 0.00216$	$0.1469 \pm 0.0004$ [131, 134]
$A_e$ (from $A_{LR}$ lep)	$0.1544 \pm 0.0060$	$0.1469 \pm 0.0004$ [131, 134]
$A_e$ (from Bhabba pol)	$0.1498 \pm 0.0049$	$0.1469 \pm 0.0004$ [131, 134]
$A_\mu$	$0.142 \pm 0.015$	$0.1469 \pm 0.0004$ [131, 134]
$A_\tau$ (from SLD)	$0.136 \pm 0.015$	$0.1469 \pm 0.0004$ [131, 134]
$A_\tau$ ( $\tau$ pol)	$0.1439 \pm 0.0043$	$0.1469 \pm 0.0004$ [131, 134]
$A_c$	$0.670 \pm 0.027$	$0.66773 \pm 0.0002$ [131, 134]
$A_b$	$0.923 \pm 0.020$	$0.92694 \pm 0.00006$ [131, 134, 135]
$A_s$	$0.895 \pm 0.091$	$0.93563 \pm 0.00004$ [131, 134]
$A_{e,FB}$	$0.0145 \pm 0.0025$	$0.0162 \pm 0.0001$ [131, 134]
$A_{\mu,FB}$	$0.0169 \pm 0.0013$	$0.0162 \pm 0.0001$ [131, 134]
$A_{\tau,FB}$	$0.0188 \pm 0.0017$	$0.0162 \pm 0.0001$ [131, 134]
$A_{b,FB}$	$0.0996 \pm 0.0016$	$0.1021 \pm 0.0003$ [131, 134, 135]
$A_{c,FB}$	$0.0707 \pm 0.0035$	$0.0736 \pm 0.0003$ [131, 134]
$A_{s,FB}$	$0.0976 \pm 0.0114$	$0.10308 \pm 0.0003$ [131, 134]
$\Gamma_W(\text{GeV})$	$2.085 \pm 0.042$	$2.0903 \pm 0.002$ [114]
$\alpha(M_Z^2)^{-1}$	127.93	$127.93 \pm 0.014$ [58]

**Table 1.** EWPO used in numerical results of this work. Experimental results are taken from Tab. 10.3 of [130]. The theory results include the full set of two-loop contributions for the  $Z$  pole observables, along with higher order corrections when known. The theory predictions are computed using the formulae in the indicated references and our input parameters as detailed in the text.

Data Group [130], while the theoretical predictions include the full set of two-loop contributions and higher order corrections when known. The theory predictions are computed using the formulae in the indicated references and the input parameters of Sec. 2.3, and the theory errors include the parametric uncertainties on the top and Higgs masses [131], along with the estimated theory uncertainties described in the respective papers.

For the FCC-ee projections, we provide the relative percentage uncertainty on Higgs production via  $e^+e^- \rightarrow Zh$ , followed by each decay channel, in Tab. 2. We consider two energy runs, at  $\sqrt{s} = 240$  GeV with statistics of  $10.8 \text{ ab}^{-1}$  and at  $\sqrt{s} = 240$  GeV with  $3.12 \text{ ab}^{-1}$  [116]. For the  $WW^*$  decays, we include the fully hadronic  $W$  decays, with the  $Z$  decaying to  $e^+e^-$ ,  $\mu^+\mu^-$  or  $\nu\bar{\nu}$ .

Tab. 3 reports the projected uncertainties on the EWPO at FCC-ee. All numbers are taken from Ref. [114], unless otherwise stated. For each observable, we detail the statistical, systematic and theoretical errors, and add them in quadrature for the results of this work. We further divide the theoretical uncertainties between those associated with the extraction of the pseudo-observables from the data at the  $Z$  pole, which requires theory inputs for instance on the simulation of radiation and modeling of hadronization and other non-perturbative effects (labeled “PO”), and those that directly come from perturbative calculations (“Theory”). We consider two possible future scenarios: a conservative one

	$\sqrt{s} = 240$ GeV	$\sqrt{s} = 365$ GeV
$b\bar{b}$	0.21	0.38
$c\bar{c}$	1.6	2.9
$s\bar{s}$	120	350
$gg$	0.8	2.1
$\tau^+\tau^-$	0.58	1.2
$\mu^+\mu^-$	11	25
$WW^*$	0.8	1.8
$ZZ^*$	2.5	8.3
$\gamma\gamma$	3.6	13
$Z\gamma$	11.8	22

**Table 2.** Uncertainty in % on Higgstrahlung measurements including Higgs decays at FCC-ee with  $10.8 \text{ ab}^{-1}$  ( $3.12 \text{ ab}^{-1}$ ) at  $\sqrt{s} = 240$  GeV ( $\sqrt{s} = 365$  GeV) [136].

FCC-ee Uncertainties	Stat	Syst	PO(C)	PO(A)	Theory (C)	Theory (A)
$\Delta\Gamma_Z(\text{KeV})$	4	12	35	—	80	16
$\delta R_e$	$3.4 \times 10^{-6}$ [136]	$2.3 \times 10^{-6}$ [136]	$4 \times 10^{-4}$	—	$1.2 \times 10^{-3}$	$2 \times 10^{-4}$
$\delta R_\mu$	$2.4 \times 10^{-6}$	$2.3 \times 10^{-6}$	$4 \times 10^{-4}$	—	$1.2 \times 10^{-3}$	$2 \times 10^{-4}$
$\delta R_\tau$	$2.7 \times 10^{-6}$ [136]	$2.3 \times 10^{-6}$ [136]	$4 \times 10^{-4}$	—	$1.2 \times 10^{-3}$	$2 \times 10^{-4}$
$\delta R_b$	$1.2 \times 10^{-6}$	$1.6 \times 10^{-6}$	$4.4 \times 10^{-5}$	$9 \times 10^{-6}$	$2 \times 10^{-5}$	$3.5 \times 10^{-6}$
$\delta R_c$	$1.4 \times 10^{-6}$ [136]	$2.2 \times 10^{-6}$ [136]	$1.7 \times 10^{-4}$	$3.4 \times 10^{-5}$	$1 \times 10^{-5}$	$2 \times 10^{-6}$
$\Delta\sigma_h(p\bar{b})$	0.03 [136]	0.8 [136]	1.7	—	1.6	0.3
$\Delta A_e$	$14 \times 10^{-6}$ [136]	$11 \times 10^{-6}$ [136]	$19.5 \times 10^{-5}$ [*]	—	$5.3 \times 10^{-5}$ [*]	$4.5 \times 10^{-6}$ [*]
$\Delta A_\mu$	$32 \times 10^{-6}$ [136]		$19.5 \times 10^{-5}$ [*]	—	$5.3 \times 10^{-5}$ [*]	$4.5 \times 10^{-6}$ [*]
$\Delta A_\tau$	$34 \times 10^{-6}$ [136]		$19.5 \times 10^{-5}$ [*]	—	$5.3 \times 10^{-5}$ [*]	$4.5 \times 10^{-6}$ [*]
$\Delta A_c$	$60 \times 10^{-6}$ [136]		$91 \times 10^{-5}$ [*]	—	$2.3 \times 10^{-5}$ [*]	$2 \times 10^{-6}$ [*]
$\Delta A_b$	$98 \times 10^{-6}$ [136]		$126 \times 10^{-5}$ [*]	—	$4.3 \times 10^{-6}$ [*]	$3.7 \times 10^{-7}$ [*]
$\Delta A_{e,FB}$	$3.3 \times 10^{-6}$ [136]	$2.4 \times 10^{-6}$ [136]	$4.3 \times 10^{-5}$	—	$1.2 \times 10^{-5}$ [*]	$1 \times 10^{-6}$ [*]
$\Delta A_{\mu,FB}$	$2.3 \times 10^{-6}$ [136]	$2.4 \times 10^{-6}$ [136]	$4.3 \times 10^{-5}$	—	$1.2 \times 10^{-5}$ [*]	$1 \times 10^{-6}$ [*]
$\Delta A_{\tau,FB}$	$2.8 \times 10^{-6}$ [136]	$2.4 \times 10^{-6}$ [136]	$4.3 \times 10^{-5}$	—	$1.2 \times 10^{-5}$ [*]	$1 \times 10^{-6}$ [*]
$\Delta A_{b,FB}$	$4 \times 10^{-6}$ [136]	$4 \times 10^{-6}$ [136]	$3.2 \times 10^{-5}$	$2.8 \times 10^{-6}$	$3.8 \times 10^{-5}$ [*]	$3.2 \times 10^{-6}$ [*]
$\Delta A_{c,FB}$	$5 \times 10^{-6}$ [136]	$5 \times 10^{-6}$ [136]	$2.3 \times 10^{-5}$	$2.1 \times 10^{-6}$	$2.9 \times 10^{-5}$ [*]	$2.5 \times 10^{-6}$ [*]
$\Delta\Gamma_W(\text{KeV})$	270	200			1000	100
$\Delta\alpha(M_Z)^{-1}$	$8 \times 10^{-4}$	$3.8 \times 10^{-3}$			$5 \times 10^{-5}$	$2 \times 10^{-5}$

**Table 3.** Projected uncertainties on EWPO at FCC-ee from Tera-Z with  $205 \text{ ab}^{-1}$  and  $\Gamma_W$  measured at the  $WW$  threshold with  $19.2 \text{ ab}^{-1}$ , from Ref. [114] unless otherwise stated. Theory uncertainties are divided into those associated with the definition of pseudo-observables at the  $Z$  peak (“PO”) and those coming from calculations (“Theory”). Both conservative (“C”) and aggressive (“A”) scenarios are considered. The dash means the uncertainty is assumed to be negligible. Numbers labeled by [\*] are found by linear propagation of errors from Ref. [114].

(“C”), where theory improvements are reached only by extending existing computational methods, and an aggressive one (“A”), where more fundamental advances in theoretical techniques is foreseen.

The dash indicates a negligible uncertainty as compared to other error sources. Entries where the information separation between “PO” and “Theory” uncertainties does not apply have been left blank, while the symbol [\*] denotes that the number has been obtained by

linear propagation of errors, following a similar approach as Ref. [137]. We denote relative uncertainties with  $\delta$  and absolute ones with  $\Delta$ .